Prompt-gamma monitoring in hadrontherapy: A review

J. Krimmer, D. Dauvergne, J.M. Létang, E. Testa

Nuclear Inst. and Methods in Physics Research, A 878 (2018) 58–73

Contents lists available at ScienceDirect

Nuclear Inst. and Methods in Physics Research, A

journal homepage: www.elsevier.com/locate/nima

Prompt-gamma monitoring in hadrontherapy: A review

J. Krimmer [a], D. Dauvergne [b,*], J.M. Létang [c], É. Testa [a]

[a] IPNL, Université de Lyon, Université Lyon 1, CNRS/IN2P3 UMR5822, F-69622 Villeurbanne, France
[b] LPSC, Université Grenoble-Alpes, CNRS/IN2P3 UMR5821, F-38026 Grenoble, France
[c] Univ Lyon, INSA-Lyon, Université Claude Bernard Lyon 1, UJM-Saint Étienne, CNRS, Inserm, Centre Léon Bérard, CREATIS UMR 5220 U1206, F-69373, Lyon, France

ARTICLE INFO

Keywords:
Particle therapy
Hadrontherapy
Prompt-gamma
Proton therapy
Gamma camera

ABSTRACT

Secondary radiation emission induced by nuclear reactions is correlated to the path of ions in matter. Therefore, such penetrating radiation can be used for *in vivo* control of hadrontherapy treatments, for which the primary beam is absorbed inside the patient. Among secondary radiations, prompt-gamma rays were proposed for real-time verification of ion range. Such a verification is a desired condition to reduce uncertainties in treatment planning. For more than a decade, efforts have been undertaken worldwide to promote prompt-gamma-based devices to be used in clinical conditions. Dedicated cameras are necessary to overcome the challenges of a broad- and high-energy distribution, a large background, high instantaneous count rates, and compatibility constraints with patient irradiation. Several types of prompt-gamma imaging devices have been proposed, that are either physically-collimated or electronically collimated (Compton cameras). Clinical tests are now undergoing. Meanwhile, other methods than direct prompt-gamma imaging were proposed, that are based on specific counting using either time-of-flight or photon energy measurements. In the present article, we make a review and discuss the state of the art for all techniques using prompt-gamma detection to improve the quality assurance in hadrontherapy.

Contents

* Corresponding author.
E-mail address: denis.dauvergne@lpsc.in2p3.fr (D. Dauvergne).

http://dx.doi.org/10.1016/j.nima.2017.07.063
Received 16 May 2017; Received in revised form 27 July 2017; Accepted 30 July 2017
Available online 12 August 2017
0168-9002/

1. Introduction

Hadrontherapy – where hadron has the meaning of light ion – makes use of the precise relation between projectile energy and energy deposition along nearly straight trajectories inside matter. This energy deposition obeys the rules of electromagnetic energy transfer during collisions with target electrons, and therefore it is maximum near the end of the ion range. This provides hadrontherapy with a high ballistic precision, both longitudinally and transversally. Although this high-technology modality reached the phase of industrial development, there is still a very large room for technical, physical and biological optimizations, and henceforth economical and medical return improvement. Physicists have to play an important role in such developments [1–4]:

- in the concept of new accelerators, that are requested to be cheaper, more compact, more intense while rapidly changing the beam energy, and with delivery modes to the patient approaching those of photon therapy (rotating gantries) or even surpassing them (fast 3D-Pencil Beam Scanning) [5],
- to help bridging a link between absorbed physical dose and tumor control probability/normal tissue complication probability [2,6],
- to help optimizing treatment planning, with faster simulations, better evaluation of the relative stopping power during planning imaging with novel tools like ion radiography or multi-energy X-ray CT, and with a better estimate of the (low) secondary doses induced by nuclear reactions,
- to help control and monitoring the beam delivery [7]: moving organs require either gating, tracking and/or repainting strategies, and thus are still difficult to irradiate efficiently. On top of that, remains the basic need to know where the beam effectively stops inside the patient body. The present paper addresses this last issue.

Actually, the high ballistic precision of hadrontherapy makes this technique quite sensitive to any source of deviation with respect to the treatment planning: patient mispositioning, organ motion or anatomic changes between fractions: tumor shrinking, weight loss, cavity filling. It is also sensitive to uncertainties in the planning itself: estimation of the tumor volume by the clinician, and, more particularly, the estimation of the tissue relative stopping power (RSP) values that are deduced from X-ray CT (*i.e.* the conversion of photon attenuation coefficients to stopping power for ions). Nowadays, safety margins are applied in the Planning Treatment Volume (PTV) in order to ensure that the Clinical Target Volume (CTV) is effectively irradiated with the prescribed dose. In proton-therapy, such margins are typically [2.5–3]% of the proton range + [2–3] mm [8]. For deep-seated tumors, this value is close to a centimeter. Another consequence is that radio-oncologists do not dare to irradiate a tumor with an organ at risk located just behind it in the beam direction. Thus, the reduction of margins would result in a reduction of the PTV – up to a certain point – and would open the possibility of additional irradiation ports when organs at risk are located nearby the tumor. Margin reductions may be obtained either by improving the precision of the treatment planning, or by controlling online the ion range, leading to heuristic improvement of the state of the art.

As the primary beam stops inside the patient, online control of the range can be performed by means of secondary radiations issued from nuclear reactions. Indeed, nuclear reactions may occur all along the projectile path, until close to the Bragg peak region when the kinetic energy falls below the Coulomb barrier. Therefore, secondary radiation emission is correlated to the primary ion range, although the underlying hadronic interaction processes differ from the electromagnetic interaction governing energy loss. Other imaging modalities appear promising in some specific cases, like ion-induced ultrasounds [9], measurement of secondary electron bremsstrahlung [10] or MRI [11] (with specific problems associated to beam bending in the patient in case of online MRI [12]). However, these techniques can be difficult to generalize.

Positron Emission Tomography (PET) consists in the imaging of the decay of positron emitters created during the fragmentation of target nuclei (any kind of particle therapy) or of the projectiles themselves (carbon or heavier ions therapy). This imaging modality has already been applied clinically online at GSI [13] and, more recently at CNAO [14]. The observation of the beta decay is delayed, with respect to the irradiation, by the lifetime of the radioactive isotopes. Therefore, even with an in-beam PET recording decays during the treatment fraction and between beam-pulse delivery periods – a necessary condition to avoid background from prompt radiations – the time requested to accumulate statistics is of the order of a minute, and therefore comparable to that of the fraction delivery. Thus PET still represents an *a posteriori* verification of the irradiated volume (see Discussion section). Moreover, metabolic washout will tend to dilute the radioisotope distribution, which, contrary to contrast agents in nuclear imaging, are not fixed on the organs of interest.

In the case of ions heavier than protons, light secondary charged fragments may be produced at typically the same velocity as the projectiles, or even faster, and thus have (i) a non-negligible probability to emerge from the patient and, even more, (ii) keep some memory of the initial interaction point within the projectile range, and therefore provide also information of the primary ion range. The detection of these secondary charged particle for the verification of carbon-ion therapy is sometimes called Interaction Vertex Imaging (IVI) [15–17]. It has been investigated both with Monte Carlo simulations and experimental studies showing that millimetric precision on ion range can be obtained in homogeneous targets at a spot scale (10^6 carbon ions) and with small particle trackers (a few centimeters in edge).

Besides auto-activation and charged-particle emission, the prompt emission of high-energy photons is expected to provide a more direct and instantaneous vision of the beam range in matter. The idea to use prompt-gamma (PG) detection to monitor ion ranges in hadrontherapy was first proposed in 2003 by Stichelbaut and Jongen at the PTCOG meeting [18]. Then a proof of principle was published by Min et al. in 2006 [19], with a collimated and shielded detector scanning proton beam ranges in a water tank. Testa et al. showed soon after that carbon ion range is also measurable, provided Time-of-Flight (TOF) is employed to discriminate PGs issued from the target from a large background of secondary radiation [20]. Since then, the topic motivated many research groups worldwide, and several different detection modalities were proposed. The aim of this article is to give an overview of such progress.

The next section will review some rationale of PG emission during hadrontherapy. The section Simulations and PG Yields presents the state of the art on models to reproduce and predict PG emission. The section Prototypes will review the various PG detection modalities that

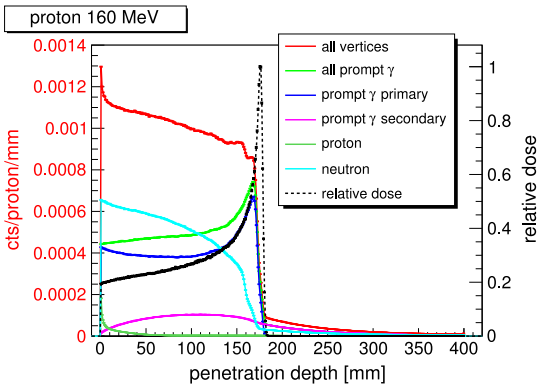

Fig. 1. Emission vertices of secondaries with energies larger than 1 MeV emerging from a water target (cylinder with 15 cm diameter, 40 cm length) irradiated by a 160 MeV proton beam.

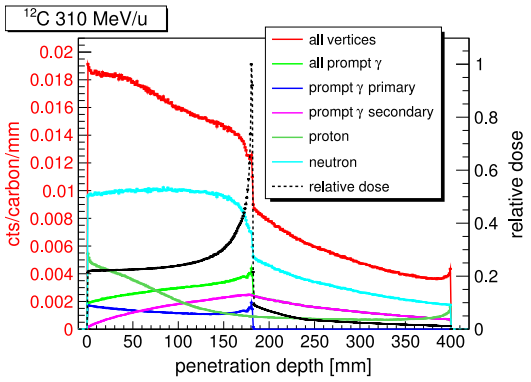

Fig. 2. Same as Fig. 1, for 310 MeV/u carbon ion beam.

have been proposed, the corresponding prototypes under development, and their reconstruction strategies or challenges. The last section will discuss about clinical applicability of PG detection, its comparison and complementarity with other modalities, and the challenges that are still faced before PG monitoring becomes widely employed in Quality Assurance systems of hadrontherapy.

2. PG features and imaging specificities

2.1. PG features

Figs. 1 and 2 illustrate the longitudinal distribution of emission vertices of prompt secondary radiation emerging from a phantom, composed of a homogeneous water cylinder of 15 cm diameter and 40 cm length. The distributions result from a Geant4.10 simulation. The cylinder is irradiated axially by protons (Fig. 1) and carbon ions (Fig. 2). The beam energies were chosen such that the range is the same in both cases. No energy spread is considered. The relative longitudinal dose profiles are also represented. For practical reasons of detectability a threshold of 1 MeV energy of particles emerging from the phantom is set. These vertex distributions correspond to nuclear reaction locations, and they are correlated to the primary ion ranges. From the present example it is clear that PGs are the best candidates for prompt radiation monitoring. Indeed, although fast neutrons vertices are also correlated to the beam range, they are very unlikely to keep the information on their initial emission direction during the traversal of the target. The distribution of protons is a bit misleading here: the particular elongated-geometry of the target makes it very unfavorable for the transmission of forward-generated protons. Therefore, the small amount of protons emerging in 4π mostly arises from vertices located close to the target entrance. For both incident beams, the prompt-gamma generation profiles are well correlated to the range. If one regards the sharpness and position of the emission falloff in the Bragg peak region, the correlation is better for carbon ions than for protons. However, note that secondary particles generate in turn ternary ones during secondary reactions, outside the primary beam path, and possibly beyond the Bragg peak. This secondary-interaction production is more pronounced for carbon than proton beams. The yield of secondary vertices increases with penetration depth, and starts to decrease beyond the Bragg peak. This decrease is quite slow, and, for the particular case illustrated in Fig. 2, the majority of PGs emerging from this phantom are generated by secondaries.

The correlation between longitudinal PG and dose profiles makes it possible to use 1D PG imaging (PGI) as a tool to retrieve the Bragg peak position, for a given beam position and energy, *i.e.* for a given pencil beam spot in case of active beam delivery, provided the available statistics is sufficient.

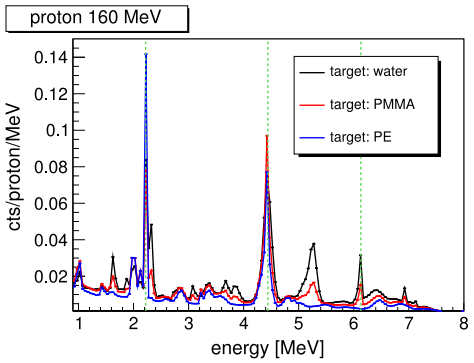

Fig. 3. Energy spectra of PG with energies larger than 1 MeV emerging from water, polyethylene and PMMA cylinders (15 cm diameter, 25 cm length) irradiated by a 160 MeV proton beam. The vertical lines mark three transitions that are discussed in the text.

A large part of the PG spectrum at emission is constituted by discrete lines, as illustrated in Fig. 3 for PG emission in water, polyethylene (PE) and polymethymethacrylate (PMMA) irradiated with a 160 MeV proton beam (Geant4.10). One can notice in particular the discrete lines coming from deexcitation of ^{16}O at 6.13 MeV and ^{12}C at 4.44MeV. Another line at 2.2 MeV is particularly pronounced for PE: it results from the deexcitation of deuterium, after neutron capture by hydrogen. This is typically a ternary photon, the distribution of which is not correlated to the primary proton range.

From the distributions of primary PG in Figs. 1 and 2, one sees that the PG yields per unit path length are almost independent on the beam energy – a slight decrease with penetration depth is due to the beam attenuation – until the very last centimeters of the range. Fig. 4 illustrates the increase of PG yields at low energies: the PG energy spectra emitted from a thin PMMA target (1 mm) are shown for three different beam energies. A global enhancement is observed as the energy decreases. Furthermore, this enhancement depends on the particular gamma-line. This property was exploited by Verburg et al. [21] to use PG Spectroscopy (PGS) as a tool to retrieve proton range and identify the traversed materials.

Finally, Fig. 5 presents the time-of-flight (TOF) spectra of PG emerging from the PMMA target (same cylinder as in Fig. 3) irradiated with 65 MeV, 100 MeV and 160 MeV incident proton beams. The origin of time corresponds to a fixed point located 2 m upstream of the target. We clearly see the influence of proton energy and therefore proton range on the PG peak position, width and integral. The idea behind PG-Timing (PGT) proposed by Golnik et al. [22] is to retrieve the beam range by means of time position and width. The PG-Peak Integral (PGPI) method proposed by Krimmer et al. [23] makes in addition use of the integral to verify the beam position, the range and thus the energy deposited in the patient, therefore approaching *in vivo* dosimetry.

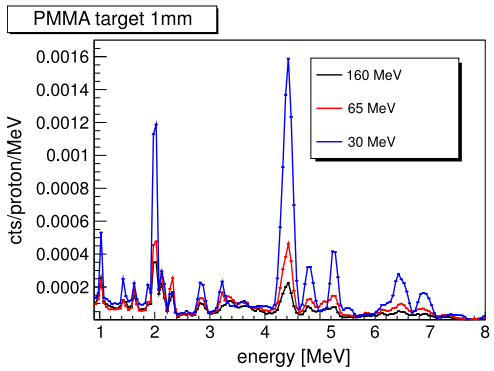

Fig. 4. Energy spectra of PG with energies larger than 1 MeV emerging from a 1 mm thick PMMA target irradiated by 30, 65 and 160 MeV proton beams.

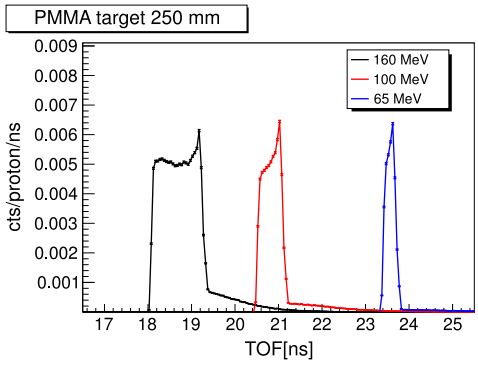

Fig. 5. Time-of-flight (TOF) spectra of PG emerging from the PMMA target with 65 MeV, 100 MeV and 160 MeV proton beams.

As explained above, not only the PG spatial distribution can be exploited to verify ion ranges during hadrontherapy but also PG energy and TOF spectra that somehow carry information on ion range.

Table 1 summarizes the various features exploited by the different PG modalities: determination of the PG position (vertex), energy or time at emission (TOF). Some features may be used as an option.

2.2. PG statistics

In order to be more general, let us give some rough but helpful figures: the PG production yields per projectile for 15 cm range in water are about 0.05 per proton and about 0.3 per carbon ion. These yields are similar for the production of β^+ emitters (altogether) [24–26]. For incident carbon ions, the secondary proton production is larger (~ 0.3 per projectile) [16,27,28].

Secondary radiation attenuation should also be considered since only a fraction of the emitted secondaries will emerge from the patient body while keeping the information on the creation vertex. For PET detection, transmission through the patient of two 511 keV photons emitted back-to-back has to be considered, which is about 5 times lower than for 1–10 MeV PGs according to [29]. Average clinical beam intensities are of the order of 10^{10} p/s and $10^7 - 10^8$ carbon/s. Regarding the number of incident ions per spot in active delivery with pencil-beam scanning (PBS), it varies by about 2 orders of magnitude. If we consider the most important spots for a 2 Gy irradiation (generally in the distal region of the PTV), the number of incident ions is around 10^8 for protons and 10^6 for carbon ions [30,31]. Thus, for these spots, a few 10^7 (resp. 10^5) PGs are available in 4π for detection in a time duration of a spot irradiation (~10 ms) during a treatment with protons (resp. carbon ions). These numbers will be reduced by the detection efficiency (including solid angle) and the possible focus on the imaging close to the falloff region.

2.3. Specificity of PG imaging

Table 2 presents the specificities of PG cameras for hadrontherapy with respect to conventional medical imaging. It is clear from these specificities that dedicated cameras are needed, with special features like high energy detection capability and count rate capability, and data acquisition systems that have to be adapted to the beam time structure.

For the particular objective of the precision for the falloff determination in the 1D-profile, the background plays a major role. Indeed, if we describe the falloff features in terms of contrast C, falloff width FW and background level B, it has been shown that the falloff retrieval precision FRP is determined by the following equation for homogeneous targets [32]:

$$FRP = \frac{\sqrt{B}}{C} = \frac{1}{\sqrt{N}} \tag{1}$$

where N is the number of incident ions. A striking result is that the falloff width has no influence on the FRP. This means that the priority when optimizing camera designs is the detection efficiency and the background rejection (shielding, TOF,...).

As we will see in Section 4, detection efficiencies of PG cameras – ranging from 10^{-5} (collimated cameras) to 10^{-4} (Compton cameras) – will lead to relatively low numbers of detected PG at spot level for pencil beam scanning systems.

2.4. Verification method

To conclude this section, the general objective of PG control of hadrontherapy would ideally be a real-time 3D verification of the dose. However, the relation between dose (by electromagnetic interactions) and PG emission (nuclear reactions) is not straightforward, and needs multi-parametric calibration: beam species and energy, target composition, detailed reaction channels (discrete lines), angular distribution, absorption, detection conditions.... Nevertheless, because of the correlation between range and PG emission profiles, range verification can be performed. As it is done with PET, this verification is obtained via a comparison between measured and predicted distributions, in accordance with the treatment planning. The next section addresses the issue of the reliability of PG predictions to meet the requirements of clinical benefits.

3. Simulations and PG yields

3.1. Simulations

Prompt-gamma monitoring during a treatment delivery relies on the prediction of the detector response. This is carried out by simulations that are based on specific DICOM[1] data (patient planning-CT volume and treatment-plan) and beam models (radiation quality). Therefore, precision and accuracy of the corresponding physical models and data in the simulations are crucial, especially since prompt-gamma production depends both on the ion energy, i.e. the position relative to the Bragg peak, and the target nucleus. The discrete excited states of the residual nuclei make it even possible to implement prompt-gamma spectroscopy to both monitor the beam range and assess the chemical composition [21].

Monte Carlo approaches. The simulation of the prompt-gamma production corresponding to a treatment plan can be very time consuming if a Monte Carlo simulation is carried out [26,33,34]. The course of actions for the acceleration of the simulations are several. A specific GPU-oriented implementation of the Monte Carlo engine highly improves the software efficiency. For example the goCMC package developed by Qin et al. under OpenCL framework (for code portability) achieved

[1] Digital Imaging and COmmunications in Medicine.

Table 1
PG modalities classified according to the PG features they exploit. Check marks in brackets mean that TOF or energy measurements are not mandatory.

PG features	Imaging systems		Non-imaging systems		
	Physical collimation	Electronic collimation	PG Timing (PGT)	PG Peak Integral (PGPI)	PG Spectroscopy (PGS)
Position	✓	✓			
Energy	(✓)	(✓)	(✓)	(✓)	✓
TOF	(✓)	(✓)	✓	✓	(✓)

Table 2
Specificities of PG cameras for hadrontherapy with respect to conventional medical imaging.

	Medical imaging	Hadrontherapy
Main objective	Activity distribution ⇒ Need for good spatial resolution	Ion range (1D profile) ⇒ Edge detection
Signal	Adjustment of injected activity Mono-energetic gamma	Driven by the dose and the accelerator (time structure) Broad energy spectrum
Main background	Compton interactions in patient Random coincidences (PET)	Neutrons and ternary radiation

clinically-acceptable dose calculation accuracy within a few tens of seconds at the expense of omitting the calculation of electron and neutron transport [35]. Giantsoudi et al. did the clinical validation of this CUDA[2] -implemented code named gPMC for proton therapy dose calculation with an efficiency of three orders of magnitude relatively to Monte Carlo typically [36].

Approximate methods such as condensed history transport (mainly for electrons) and basic Variance Reduction Techniques (VRT) are already implemented in most MC simulation packages to increase the calculation efficiency [37]. VRT are also extensively applied, making use of existing techniques such as Russian roulette, splitting or interaction forcing to speed up the calculations. To give reasonable execution times for in-beam PET calculations, Sommerer et al. had to introduce new PET-specific VRT [38], among which β+-active residual nucleus replication and direction biasing for annihilation photons. The track-length estimator developed initially for dose calculations under kerma approximation [39] has also being translated to the simulation of positron emitters [40] and prompt-gamma production [41,42]. In particular El Kanawati et al. [41] and Huisman et al. [42] have shown that computation times can be reduced by about three orders of magnitude, which enables predicting the entire 3D map of the prompt-gamma spectrum related to the distal energy layer of a treatment plan within a couple of hours on a single core computer. This is still not sufficient for direct translation to clinic but makes it conceivable.

Analytic approaches. Beside accelerating Monte Carlo engines, the implementation of an analytic model using ray-tracing is mostly efficient [43,44]. In analytic approaches, prompt-gamma emission profiles are usually precomputed with Monte Carlo simulations (eg Penelope PENH in [43]), and scored in tables, additionally getting proton differential cross-section data from ICRU report No. 63 [45]. The ray tracing is not necessarily linear, Sterpin et al. proposed for example a depth-varying curvilinear ray tracing in the CT geometry to model the spot size and shape [43]. Pencil beam algorithms based on measured yields [46] or measured activities [47] have also been developed for the calculation of positron emitter distributions.

Imaging device modeling. The modeling of the prompt-gamma detection by the imaging device can be implemented using standard convolution approaches as proposed by Sterpin et al. [43], where filtering of the emission profile is carried out using a transfer-function kernel fit from precomputed MC simulations. This type of methods based on convolution is sometimes coupled to the force-detection variance reduction technique as de Jong did for SPECT [48]. Beside convolution, the angular response function (ARF), widely used for gamma-camera modeling [49], is also an appropriate alternative to model the detector response in MC calculations.

[2] Compute Unified Device Architecture (Nvidia).

Filtering approaches. Instead of precomputing reference prompt-gamma emission profiles, filtration of the dose distribution maps (already available from the TPS) makes it possible to directly get the expected prompt-gamma distribution [50], or β+ emitters [51–53]. This eludes the modeling of the beam model in the Monte Carlo source setup [54]. The great advantage of such filtering-based approaches is the ability to pose the inverse problem: the calculation of the dose from the detected prompt-gamma distribution. An evolutionary algorithm has recently been proposed by the Dresden-Rosendorf group to solve this issue [55].

Models. When benchmarking various Monte Carlo codes and existing evaluated data, we may find large differences in the prompt-gamma production depending on the target and the gamma-line under consideration [56,57,34,58]. In all cases, a fine tuning of the nuclear model parameters has to be carried out since most Monte Carlo toolkits were not specifically developed for the energy range related to hadrontherapy applications. For example, large improvements of the Geant4 hadronic models have been obtained by Dedes et al. when decreasing the width of the Gaussian wave function in the quantum molecular dynamics (QMD) model [59]. Quantitative characterization of prompt-gamma emission yields have been recently performed [34,25,60] but more work remains to be done in terms of hadronic models development and differential cross-sections and prompt-gamma yields measurements in the clinical energy range used in ion therapy [58,3].

Reconstruction. As regards the reconstruction of prompt-gamma distributions, the complexity of the algorithm depends on the camera design. Multi-slit cameras [61], which already provide the coordinate of the prompt-gamma production site along the beam direction, can be coupled to the transversal coordinates of the beam (via the beam monitor or hodoscope [62,63]), which makes the reconstruction algorithm trivial. For more complex setup designs like Compton cameras, specific reconstruction methods have to be developed. For a Compton camera, the location of the prompt-gamma production site lies on a cone, whose angle is unique provided the scattered photon is totally absorbed in a two-event scenario (*i.e.* based on a single Compton scattering) or just partially absorbed in scenarios with two or more scattering events. It can be further reduced to a portion of a cone if the recoil Compton-electron is tracked [64], and total photon absorption is no longer required eventually in that case. In practice, the cone must be thickened to take into account the uncertainties in the cone apex location, the scattering angle and (if available) the scattering plane. The easiest technique making use of the transversal position of the beam is to implement a geometrical line-cone reconstruction [65]. Maxim et al. showed that the inversion of the Compton transform translates to an analytic filtered backprojection (FBP) algorithm [66], very similar in essence to standard FBP in X-ray cone-beam computed tomography. It is fast but the main drawback of it is its sensitivity to the projection

truncation issue and its inability to deal with complex acquisition designs. A more versatile alternative is the iterative methods, like the Maximum Likelihood Expectation Maximization (MLEM) algorithm [67,68] or the origin ensemble [69–71] based method, which requires the computation (on-the-fly or pre-calculated) of a large probability system matrix. Recently, Gillam et al. proposed a 3D-spectral reconstruction in Compton imaging [72,73], making it possible to increase the detection sensitivity by using two-event coincidences, extending the 3D image-space over the range of possible incident energies. Gillam et al. used the standard MLEM algorithm to compute the distribution of prompt-gamma production [72] but more recently stochastic origin ensembles have also been proposed in Compton imaging for homeland security applications [74] to localize and identify the source at the same time.

3.2. PG yields

Although some data exist for the production of PG by proton or carbon ions for general nuclear physics and astrophysics purposes (see e.g. [75,76] and references therein), specific data are needed for hadrontherapy, where specific energies, thick targets and mixed fields are involved. An Italian collaboration performed several measurements of PG yields with carbon ions in PMMA targets, Agodi at 80 MeV/u [77,78] and Mattei at 220 MeV/u [79]. More recently [80], with the same detectors, they measured yields for ^{4}He, ^{12}C and ^{16}O ion beams at various energies (target ranges between 3 and 13 cm), at 60° and 90° observation angles. Minor effects were observed for the two angles, and their results are in agreement with data from different experiments [78,81]. A universal behavior as function of specific kinetic energy was observed for the various projectiles. However, proton yields may not follow this behavior (this was not tested in this paper).

Pinto et al. re-evaluated the results obtained by our FP7 collaboration [81] as a compilation of single slit experiments at 90°, with 75 MeV/u, 95 MeV/u and 310 MeV/u carbon ions, and 160 MeV protons, with PMMA targets (and one measurement with water target). The main prompt-gamma yields per incident ion, per millimeter and per steradian are equal to: $(124 \pm 0.7_{stat} \pm 30_{sys}) \times 10^{-6}$ for 95 MeV/u carbon ions, $(79 \pm 2_{stat} \pm 23_{sys}) \times 10^{-6}$ for 310 MeV/u carbon ions, and $(16 \pm 0.07_{stat} \pm 1_{sys}) \times 10^{-6}$ for 160 MeV protons.

Verburg et al. [82,21] used a single-slit collimation, high-resolution $LaBr_3$ detector with Compton rejection and measured individual PG lines as a function of penetration depth in several materials. These yields are used to establish an unequivocal relation between target composition and proton range (see section Prototypes).

Recently, Kelleter et al. [60] measured quantitative production yields of the two main PG lines (6.13 MeV of ^{16}O and 4.44 MeV of ^{12}C nuclei) produced by 70 MeV and 130 MeV protons in graphite, PMMA and POM ($(CH_2O)_n$) targets with a single-slit collimated high resolution Ge detector located at 90° and 120°. The absolute yields per unit path length and unit solid angle were measured as a function of penetration depth, and compared with fits from literature data and TALYS[3] model.

Although nuclear physics models were considerably improved, the prediction of PG distribution in clinical routine still requires more accurate and precise data via comprehensive measurements.

4. Prototypes

After the suggestion to use prompt-gamma rays for monitoring purposes during hadrontherapy [18], different approaches for the realization of clinical prototypes have been followed. As summarized in Table 1, the systems can be classified in PG Imaging devices (collimated) and integrated yields counting devices (non-imaging systems). PGI devices can be further divided into systems using mechanical and electronic (Compton cameras) collimation, respectively. Uncollimated systems will use additional information such as photon energy or timing.

4.1. Imaging systems

4.1.1. Mechanical collimation

Feasibility studies. The first feasibility study has been performed by Min et al. with a single detector behind a collimator with a parallel slit geometry [19]. In this case the collimator has been designed to moderate and capture fast neutrons, as well as to prevent unwanted prompt gamma rays to reach the scintillation detector. Measurements have been performed with 100–200 MeV protons. The longitudinal prompt gamma-ray profile has been obtained via a scan of the target in front of the collimator-detector arrangement. These first studies showed a correlation of the prompt gamma-ray distribution with the distal fall-off region [19]. With a similar setup and a 38 MeV proton beam it has been claimed that the distal dose edge might be determined from the prompt gamma-ray distribution within 1–2 mm [83].

In the case of carbon-ion beams neutron production is more pronounced and the discrimination against prompt gamma-rays is an issue. For this purpose time-of-flight (TOF) information can be used which also allows a reduction of neutron shielding [20,84,85]. Measurements have been performed by our collaboration with a 73 MeV/u carbon-ion beam in GANIL.[4] Due to the time structure of the accelerator (bunch width 1 ns, bunches every 80 ns) the high frequency signal of the accelerator has been used as reference for the TOF measurements. A good correlation between the prompt gamma-ray profile and the carbon ion range has been found, showing that via prompt gamma-ray measurements, a real-time control of the range is feasible in ion therapy [20,84]. Further experiments with 95 and 305 MeV/u carbon ions and PMMA and water targets showed that the prompt gamma-ray distributions were correlated to the corresponding ion ranges, whereas the neutron component did not show such a correlation [86].

PMMA targets with inserts of different densities have been used to mimic lung or bone contributions. The experiments with 95 MeV/u carbon ions revealed a difference in the detected prompt gamma-ray count rate at the insert position. Furthermore, the inserts also lead to a change in the ion range, depending on the density. A change in the ion range on the order of 1–2 mm, caused by the inserts, could be detected [81].

Parallel multislit. A clinical prototype based on parallel slit collimators will require multiple detectors or position-sensitive detectors behind the collimator. Optimizations of the collimator design have been carried out via MCNPX simulations by Min et al. [87] and Geant4 simulations by Pinto et al. [88]. The optimization is always a trade-off between efficiency and spatial resolution. In [88] two different geometries have been extracted, corresponding to two different end-points.

In a multi-slit multi-detector configuration, inter-detector scattering might occur, leading to a dilution of the measured signal. For a quantification of this contribution, dedicated measurements and simulations have been performed. It turned out that this part is on the order of 10% for 5 mm slab LYSO detectors, and can be rejected electronically, if necessary [61].

In a regular treatment with active beam delivery and pencil beam scanning (PBS) the maximum number of protons for a single spot is on the order of 10^8 [54,89]. This number also determines the number of prompt gamma-rays available for monitoring purposes. Performance tests with a small individual detector and 160 MeV protons impinging on a PMMA target have been performed. The range retrieval precision as a function of the number of incident protons has been extracted and extrapolated to a clinical size prototype detector. For such a geometry and 10^8 incident protons, a range retrieval precision on the order of 1–2 mm (RMS) is expected [32]. The use of TOF increases the signal-to-background ratio, which, in turn, could improve the precision value by a factor equal to the square root of the background reduction factor (see Section 2.3).

[3] http://www.talys.eu.

[4] Grand Accélérateur National d'Ions Lourds in Caen, France.

Pinhole/knife edge cameras. The principle of the pinhole camera, known from classical optics, can also be adapted for prompt gamma imaging. The thickness of the enclosure and the shielding need to be adapted for the prompt gamma-ray energies of several MeV. After optimization via Monte Carlo simulations, a first experiment has been performed by Kim et al. at a 50 MeV proton beam impinging on a water target [90]. The prompt gamma rays were detected with a CsI(Tl) scintillation detector behind a pinhole aperture, located to view the endpoint of the proton range [90].

The pinhole configuration allows in principle 2-D images of the prompt gamma distributions. For the purpose of range monitoring, however, the 1-D projection along the beam axis is sufficient. This changes the pinhole aperture to a single slit of the knife-edge type [91]. The geometry was optimized via MCNPX simulations and a prototype including a position sensitive detector (HiCam) was constructed by a collaboration between IBA and Politecnico-Milano [89,92]. Test measurements with 100 and 160 MeV protons showed that with a such a configuration a 1–2 mm standard deviation in the range estimation can be achieved. The corresponding doses in a homogeneous PMMA target were 15 and 25 cGy for 100 and 160 MeV, respectively [92].

In order to be compatible with count rates occurring at clinical beam currents (several nA at the nozzle), a second prototype has been constructed where the detection part consists of scintillation detector slabs (LYSO) read out via silicon photomultipliers [93]. Data were acquired with 100, 160 and 230 MeV protons impinging on a homogeneous PMMA target. A precision (2 sigma) in shift retrieval of 4 mm was reached for 0.5×10^8, 1.4×10^8 and 3.4×10^8 protons at 100, 160 and 230 MeV, respectively [93]. In inhomogeneous targets with inserts of tissue equivalent material, for most cases range deviations can be detected within less than 2 mm [94]. For range detection in the vicinity of low-density regions a penetration of the beam 7 mm after the cavity is required [94]. Such a case could be relevant for the detection of cavity filling.

In the case of laterally inhomogeneous targets range mixing occurs and the detected range deviations depend strongly on the target composition [95]. As additional information the distal slope of the detected prompt gamma distribution can be used in order to reveal the origin of the range deviation [95].

The knife-edge camera was originally developed for active beam delivery with pencil beam scanning (PBS). In clinical routine also passively scattered protons in combination with a patient specific aperture are in use. In the latter case the neutron contribution is higher than with PBS. For the knife-edge camera the prompt-gamma part is obtained via the difference of measurements with open and closed collimator, respectively. On the way towards clinical application it has been shown that the usage of the knife-edge camera is also possible for passive beam delivery and that shifts in the proton range on the order 2–5 mm can be visualized [96]. It has been further demonstrated that the neutron contribution is mainly coming from the beamline so that the background measurements with closed collimator can also be done with a water phantom, instead of the patient. When the timing information of the modulator wheel is correlated to the detector data, the acquired signal can be mapped to different anatomical regions along the beam path, which could give additional information about the source of a potential range shift [96].

Prompt gamma-ray imaging with a knife-edge camera has been applied for the first time clinically for a treatment of a head and neck tumor [97]. The measured inter-fractional global range variations were in the order of ± 2 mm which is in agreement with CT information (variations on the order of 1.5 mm). Recently, a second IBA-prototype was tested with PBS at Philadelphia [98].

Ready et al. designed a 2-D arrangement of knife-edge slit collimators which serves as coded mask aperture, and allows 2-D images of prompt gamma-ray distributions [58,99]. Behind the collimator a 4 × 4 array of streaked LSO scintillation crystals was placed. Each crystal was read by 4 photomultipliers which allowed the reconstruction of the hit (pseudo)pixel via a center of gravity method. In total more than 2000 (pseudo)pixel were present. Measurements have been accomplished at a 50 MeV proton beam impinging on a homogeneous PMMA target. The images were reconstructed via a maximum likelihood expectation maximization (MLEM) algorithm. 2-D prompt gamma-ray distributions were acquired, a Bragg peak localization with a precision of 1 mm (2σ) was obtained with $(1.7\pm0.8)\times10^8$ incident protons [58]. If one compares this camera with single knife-edge devices the improvement in terms of efficiency, field of view, 2D imaging, is at the expense of reconstruction time, *i.e.* a loss of real-time information. This will be also the case for Compton cameras described in the next section.

4.1.2. Electronic collimation: Compton cameras

In comparison to the previously described systems with passive collimation, the use of electronic collimation, i.e. Compton cameras, has the general advantage of a higher detection efficiency. Compton cameras for medical imaging have first been proposed in [100]. The principle is to use successive interactions (two or more) of the incident photons in segmented detectors. From the interaction points in the detectors and the deposited energies the direction of the incident photon can be restricted to a cone, via the application of Compton kinematics. The vertex of the photon generation is then obtained via the superposition of multiple cones. An advantage of Compton cameras is, that in principle 3-D information is available. This type of cameras is also well adapted for the purpose of prompt gamma-ray detection, as in the relevant energy range of several MeV Compton scattering is the dominant process.

The simplest realization of a Compton camera requires two detection stages, a scatter detector and an absorber. As for the monitoring purpose during hadrontherapy the energy of the produced prompt gamma-ray is *a priori* not known, this type of cameras requires a total absorption of the scattered photon in the absorber in order to kinematically reconstruct the event. Algorithms have been developed which make use of the elemental composition of the target to constrain the energy of the generated prompt gamma-rays to a few discrete lines [101,102]. Another alternative is the registration of three interactions in the detectors, which completely defines the kinematics of the incident photon but with the drawback of a reduction of the efficiency by at least an order of magnitude [103].

The detector types which have been considered for the various prototypes comprise scintillators ($LaBr_3$, LSO, BGO), semiconductors (Si, CZT) and gaseous detectors (TPC). In the following, the different systems are classified according to the used detector types and their combination.

Scintillators. A monolithic $LaBr_3$ crystal was coupled by Llosá et al. to a SiPM-array for performance tests [104] including the 3-D reconstruction of the impact position in the detector [105]. An intermediate prototype including one $LaBr_3$ and one LYSO layer [106] served for the assessment of an image reconstruction algorithm [72]. The final prototype consists of three layers of monolithic $LaBr_3$ crystals with entrance surfaces of 27.2×26.8 mm^2 and 32×36 mm^2 and thicknesses of 5 and 10 mm, respectively [107]. After successful reconstruction of point-like sources [107] tests at a 150 MeV proton beam showed that with the reconstructed Bragg peaks shifts within 10 mm can be observed [108].

A handheld Compton camera based on pixelated Ce:GAGG scintillators was constructed by Kishimoto et al. [109]. Besides medical applications such a type of camera can also be used to identify environmental radiation hotspots. The spatial resolutions for point-like sources were below 7 mm (FWHM) [109]. A first test with this device was performed at a 70 MeV proton beam impinging on water, $Ca(OH)_2$ and PMMA targets [110]. To reduce the uncertainties in the determination of the Bragg-peak location, a prototype with higher resolution is foreseen [110].

Combination semiconductor and scintillator. The concept of a combination of double sided silicon strip detectors (DSSD) as scatterers and a scintillation detector as absorber has been studied in [103,111] by our collaboration. In the case of hadrontherapy the direction of the incident ion can be exploited to reduce the reconstruction problem to line-cone intersections. In the present project, the measurement of direction of the incident ion is provided by a beam-tagging hodoscope [63]. As mentioned above, a high probability for a deposit of the total energy in the detectors is of importance for a two-stage camera. For an optimization of the absorber, different scintillators with high photo-absorption cross sections have been simulated, which resulted in optimum thicknesses of 4 and 4.5 cm for LYSO and BGO, respectively [112]. The DAQ system based on μTCA [113] comprises ASICS for the front-end electronics of the hodoscope [114] and the DSSD [115]. The prototype will consist of seven planes of DSSD ($90 \times 90 \times 2$ mm^3, 2×64 strips) and 100 BGO blocks ($38 \times 35 \times 30$ mm^3) as absorber. Individual components have been characterized, including the streaked BGO crystals with 8×8 (pseudo)pixels [116].

A reduced thickness of the scatter detectors allows the tracking of the recoiling electrons after a Compton interaction. With this information the direction of the incident photon can be confined from the full cone to an arc [117]. The complete system developed by Thirolf et al. consists of six planes of DSSD ($50 \times 50 \times 0.5$ mm^3, 2×128 strips) and a monolithic $LaBr_3$ scintillator crystal ($50 \times 50 \times 30$ mm^3) as absorber [118]. The scintillator is read via a multianode PM (H9500), the impact position is obtained via an algorithm based on the k-nearest neighbor method [119]. Test measurements with the absorber resulted in a relative energy resolution of 3.8% (FWHM) at 662 keV and a timing resolution of 270 ps [120]. Besides the here discussed monitoring purposes during hadrontherapy, Compton cameras might also be introduced to nuclear medicine. Of particular interest are new radiotracers based on β^+ emitters with a coincident γ transition. The detection of the resulting three gamma-rays allows a sub-millimeter image reconstruction where only 40 intersections are required [121].

In addition to the previously discussed silicon detectors, Cadmium Zinc Telluride (CZT) is used for various Compton camera prototypes. A CZT detector ($20 \times 20 \times 5$ mm^3, 16 cathode + 16 anode strips) as scatterer in combination with a streaked LSO crystal ($52.7 \times 52.7 \times 20$ mm^3) as absorber has been investigated by Kormoll et al. [122]. Individual components were tested with bremsstrahlung photons (up to 13 MeV) from the electron accelerator ELBE [123], which is, due to its bunch width of 5 ps, perfectly suited for timing measurements. The CZT detector showed a time resolution of 2.8 ns (FWHM), for the LSO detector this value went down to 0.6 ns (FWHM) after the application of a pixel delay calibration and a time walk correction [123]. BGO is also an interesting alternative, albeit less performant than LSO, due to its lower price and the absence of internal radioactivity [124]. The impact position at the streaked BGO crystals is obtained from the relative intensities measured at the four light sharing photomultipliers. Automated segmentation is done with the neighbor standard deviation algorithm [125]. A prototype configuration of a Compton camera, consisting of a CZT detector and three BGO crystals ($52.7 \times 52.7 \times 20$ mm^3, 8×8 pseudo-pixel), has been tested with mono-energetic 4.44 MeV photons [126]. The later were produced at a 0.9 MeV proton beam via the proton-capture resonance reaction ^{15}N(p, $\alpha\gamma$)^{12}C. The CZT detector has a relative energy resolution of 3.5% (FWHM) at 511 keV. For the BGO detectors an energy calibration for each pixel is necessary [124], and an energy resolution of 27% was found [126]. With this prototype also the feasibility of imaging the localized 4.44 MeV γ-emission region and a lateral displacement of the source (w.r.t. the camera) was proven.

An alternative method, named Gamma Electron Vertex Imaging (GEVI) has been studied by Kim et al. via simulations [127]. The concept is to convert the prompt gammas to electrons which are then tracked. A prototype has been constructed [128]. It uses a 1 mm Be plate as converter which is a compromise between favoring Compton scattering with respect to other processes like pair creation, and limiting electron multiple Coulomb scattering. The electron tracking hodoscope consists of two layers of DSSD (2×16 strips) with a surface of 50×50 mm^2 and thicknesses of 150 and 300 μm for the first and second layer, respectively. A plastic scintillator ($100 \times 100 \times 20$ mm^3) serves as calorimeter to measure the kinetic energy of the electrons. For the registration of a valid event a coincident signal from the three detection layers is required. The components have been characterized and calibrated via β- and γ-sources. Imaging of electrons has been tested with a ^{90}Sr source replacing the converter. After line backprojection the resolution of the imaged point source resulted in 16 mm FWHM. With the inclusion of the converter and gammas from a ^{60}Co source a resolution of 35 mm FWHM was obtained. The capability of imaging prompt gamma-rays from 45 MeV protons imping on a PMMA target has been demonstrated [128]. A sensitivity of 4×10^{-8} was obtained. In a future prototype the DAQ system will be replaced, which currently limits the coincidence rate to 200 Hz.

Semiconductors. Developments of Compton cameras based on semiconductor detectors, only, have been started by Peterson et al. with simulations for a three-stage system with Ge-detectors [129]. Different detector materials have been studied [130] and the influence of Doppler broadening has been investigated for HPGe and CZT detectors [131]. A prototype with four pixelated (11×11 pixels) CZT detectors has been constructed [132]. The detectors have a size of $20 \times 20 \times 15$ mm^3 and $20 \times 20 \times 10$ mm^3, respectively. At 662 keV the energy resolution amounts to 9.7 keV (FWHM). The absolute efficiencies for double and triple scatter events have been measured with the gammas from a ^{60}Co source, they result in 2.2×10^{-5} and 5.8×10^{-7}, respectively [132]. For the image reconstruction a stochastic origin ensemble (SOE) algorithm is applied, which leads to a position resolution of 2 mm [69]. With this prototype tests have been performed at clinical proton beams with 114 and 150 MeV incident energy, impinging on a water target [70]. 2-D images of the prompt gamma-ray distributions have been reconstructed. For the 1-D profiles the detection of 3 mm shifts (accuracy 1.5 mm) of the fall-off position, at an applied dose of 400 cGy, was reported [70].

New techniques have been developed for an improvement of the spatial resolution [102]. The methods comprise filters, named distance-of-closest approach (DCA) and Compton line (CL) filter. Measurements with point sources of ^{22}Na, ^{137}Cs, ^{60}Co and the prototype described in [132] have been done. The purpose of the filters is to determine the initial gamma energy and to remove "bad" interactions from the data sample. The spatial resolution is improved from 5 mm (raw data) to 2 mm or better than 2 mm with the application of the DCA and DCA + CL filters, respectively [102].

Gaseous detectors (TPC). An electron tracking Compton camera (ETCC) has been developed by Takada et al. for the detection of cosmic and atmospheric gamma rays during balloon experiments [133]. The system consists of two parts, a gaseous time projection chamber (TPC) for the electron tracking, and scintillation detectors for the registration of the scattered photons. The TPC ($10 \times 10 \times 15$ cm^3) is filled with a mixture of Argon and C_2H_6 (ratio 9 to 1) at a pressure of 1 atm. The electrons are registered in a micro-pixel chamber (μ-PIC) [134]. The scattered photons are detected in GSO:Ce pixel scintillator arrays (pixel size $6 \times 6 \times 26$ mm^3) coupled to the 64 channel multi-anode PMs (H8500). The TPC provides the 3-D information of the electron track. In combination with the data from the scintillators, the direction of the incident photon can be confined to a small arc of the Compton cone. The ETCC has been used for test measurements with a 140 MeV proton beam impinging on a water target [135]. 2-D images of the prompt gamma distributions have been extracted, revealing a correlation with the Bragg peak position. The efficiency of the used system has been determined to 3×10^{-6} [135], an improvement is expected with the usage of CF_4 in the TPC [136].

Various concepts and strategies have been used for the development of Compton cameras. Small and large prototypes have been constructed, or are still under construction, which have a very large range of efficiencies, from $\sim 10^{-8}$ up to $\sim 10^{-4}$. Still these cameras are facing

several issues: i—the coincidence detection is perturbed by fortuitous events: as pointed out by Ortega et al. [73], Ley [137] and recently by Rohling et al. [138], the beam intensity needs to be reduced in order to minimize the probability of coincidence events generated by several ions incident during the camera time-resolution window, ii—the cost of a Compton camera device may not be much smaller than that of a PET system. However, Compton cameras should not be discarded, as reconstruction tools are rapidly evolving and may help solving the first issue, and as they may provide higher efficiency and spatial resolution, with 3D capability, than collimated devices. This field is still in progress.

4.2. Non-imaging systems

Important criteria for clinical systems are also a minimization of the expenses and the footprint in the treatment room. These points are fulfilled for uncollimated systems, described in this section. The two methods, named prompt gamma timing (PGT) and prompt gamma peak integral (PGPI) are both based on TOF information obtained with scintillation detectors.

4.2.1. PGT

Proton beams entering material cause the emission of prompt gamma-rays along their path, until they are stopped. The transit time for protons with a range of 5–20 cm is on the order of 1–2 ns. As the transit time depends on the range, this information is reflected in the width of prompt gamma-ray TOF distributions. This alternative range monitoring method has first been investigated by Golnik et al. with 150 MeV protons impinging on a graphite target [22]. A change of the target position led to a change of the mean value in the TOF spectrum (see Fig. 5). Furthermore, protons traversing targets with increasing thickness from 5 to 15 cm caused a broadening in the measured TOF distributions which could be reproduced by simulations. A similar behavior was observed for an increase of the incident energy from 50 to 230 MeV which corresponds to a change in the range from 2 to 17 cm. Finally, the effect of bone and air inserts has been simulated [22].

During measurements with heterogeneous targets [139] it has been found that the phase of the RF signal, which has been used as time reference, was not stable on the time-scale of hours. These drifts cause a change of the mean TOF values on the order of 100 ps, the same order of magnitude as a shift of the target position by a few centimeters would provoke. For a monitoring and a possible correction of these phase shifts a beam monitor has been developed [140]. The principle is the coincident detection of elastically scattered protons from a thin (1 mm) PMMA target. Detectors of the phoswich type with a plastic scintillator coupled to a BGO crystal have been used. The bunch structure of the clinical cyclotron at Oncoray-Dresden, with a maximum proton energy of 230 MeV, has been characterized. For these type of accelerators the energy selection is based on degradation in an upstream part of the beamline. The resulting bunch width at the treatment or experimental area, caused by energy straggling, depends on the selected energy and the distance after the degrader. For the example given in [140] the bunch width decreases from 1.8 to 0.23 ns for an increase in energy from 69 to 225 MeV. Momentum limiting slits can be closed for a reduction of the bunch width, *e.g.* from 1.4 to 0.6 ns at 110 MeV. The transmission, however, is then reduced by a factor 10 which has a direct influence on the treatment time of patients and which would also cause an activation of the energy selection system of the beamline.

With the technique of PGT range shifts of 5 mm in homogeneous targets can be detected for clinical relevant doses, this value is reduced to 2 mm for higher statistics [139]. In ideal cases with a small bunch width, the influence of inserts of bone equivalent material is directly visible in the prompt gamma-ray distributions. A PMMA target with air cavities and an insert of bone equivalent material has been scanned perpendicular to the beam axis, the corresponding 2-D distribution reveals an excess or a diminution of the prompt gamma count rate at the positions of the inserts, w.r.t. the surrounding material [140].

The relation between an excess in the proton range and a shift of the centroid in the TOF distribution is on the order of 50 ps/cm [139]. For design considerations of a clinical system it has been estimated that 10^4 prompt gamma-rays need to be detected to spot 5 mm range shifts, even in the worst case (energy degraded to 70 MeV) with a bunch width of 2 ns [141]. Count rate estimates in combination with the above mentioned measurements show that a 2 inch detector (thickness 1–2 inches) at a distance of 30–50 cm detects enough prompt gamma-rays for a single spot in PBS. A challenge is the handling of a data throughput greater than 500 kcps. Tests have been performed with 2 inch $CeBr_3$ scintillators read via photomultiplier which are directly coupled to a U100 spectrometer. With energy-selected gamma-rays of several MeV, a timing resolution of 200 ps has been obtained at throughput rates greater than 600 kcps without losing spectroscopic performance [141].

4.2.2. PGPI

The peak integrals of prompt gamma-ray TOF distributions have been exploited by Krimmer et al. in [23]. Prior to these studies a correlation of the ambient dose in the ophtalmic treatment room at CAL-Nice (passive beam delivery) with the monitoring units (MU) from the beam delivery system has been found [142]. TOF provides a possibility for a discrimination of the prompt gamma-rays produced in the target (patient) from those generated in the beamline, *e.g.* in the nozzle. The general goal is to detect deviations from the prescribed treatment and in particular to avoid severe overdosage [143]. A system detecting prompt gamma-rays generated in the patient provides an additional safety aspect as this information is independent from other monitoring elements in the beamline.

Test measurements have been performed at a clinical cyclotron with 65 MeV protons, intensity 3×10^9 p/s, impinging on a homogeneous PMMA target. Prompt gamma-rays were registered with a cerium doped $LaBr_3$ scintillator ($25.4 \times 25.4 \times 72.2$ mm^3) read out via a dedicated DAQ card. This card allows a data throughput of several 10^5 cps with up to three detectors connected. An external signal, *e.g.* the accelerator RF or a beam monitor, serves as time reference for the TOF determination. In the case of passive beam delivery with a modulator wheel, the data can be synchronized to the position of the modulator. The measurements revealed a variation of the PGPI with the position of the modulator wheel, in accordance with simulations. With 10^8 incident protons and detectors covering a solid angle of 25 msr (which corresponds to 3–4 inches in diameter at a distance of 50 cm from the beam axis), deviations of a few per cent in the registered prompt gamma-ray count rate can be found. In the case of 65 MeV protons this corresponds to the possibility of the detection of a 3 mm range deviation in PMMA (assuming beam intensity variations are controlled at the required precision).

The effect of absorption in the target is on the same order of magnitude as possible deviations from the prescribed treatment to be detected. The combination of signals from multiple detectors placed around the target has been explored via simulations. From the ratios, information about the target position can be obtained, whereas the (geometric) mean is independent on the actual position [23].

4.2.3. PGS

An alternative and less direct method for range monitoring is also based on the identification of characteristic prompt gamma-ray lines and their relative contributions [57]. Verburg et al. performed measurements with an actively shielded cerium doped $LaBr_3$ detector. They showed that the analysis of the energy spectra at a single measurement position relatively close to the end of the beam range provides information about the target (tissue) composition (see Fig. 3), as well as on the residual proton range, via the energy dependence of the cross sections (see Fig. 4) [82,21]. This method, called Prompt-Gamma Spectroscopy (PGS) is particularly interesting, but still has to face the issues of available statistics per PG line, and the presence of mixed-beams with heterogeneities.

For proton therapy with passive beam delivery the spread out Bragg peak (SOBP) is produced by a rotating range modulator wheel. A method has been proposed at MGH to use measurements with a single collimated detector aiming close to the end of the SOBP which will reveal a correlation of the time patterns of the emitted prompt gamma-rays with the residual proton range [144]. Simulations with TOPAS resulted in an accuracy of 2 mm for the determination of the proton range in a water phantom with an applied dose of 2.5 cGy and a full-ring detector. For the case of a prostate cancer treatment a 4 mm accuracy was achieved via the simulations, with 15 cGy applied dose [144]. This proposed method was verified experimentally [145] with a single scintillation detector behind a lead shielding. The prompt gamma-ray detector was synchronized with the rotating modulator wheel to determine the relation of the prompt gamma emission from the distal part of the target and the proton range. A water phantom and an anthropomorphic phantom were used as targets. Range shifts were detected for applied doses of 30–50 cGy (RBE) with a standard deviation of 0.1–0.2 mm [145].

The energy spectra of the emitted prompt gamma-rays have been studied by Polf et al. for different targets via simulations and via measurements with Ge detectors [146,147]. The characteristic lines from ^{12}C and ^{16}O at 4.44 and 6.13 MeV, respectively, could be identified. A quantitative analysis of these lines allows for a quantification of the relative content of these isotopes in a target [148]. Absolute yield measurements by Kelleter et al. for these two particular gamma-lines have been described in Section 2 [60].

4.3. Comparison of different systems

Attempts to compare several detection systems have been published.

Smeets et al. performed experiments with 100, 160 and 230 MeV protons, in order to compare the performances of knife-edge and multi-slit collimated cameras, with the criterion of the same mass of collimator and the same volume of detector [149]. This comparison is slightly biased by the fact that the Knife-edge camera geometry was optimally designed [89], whereas the multi-collimated one was not optimized. However, the two cameras performances were very close.

In the same way, Lin et al. [150] performed GATE/GEANT4 simulations to compare the IBA knife-edge camera to a multi-slit camera as evoked by Gueth et al. [151].

In this section we reviewed the systems that have been developed (or still are under development) for PG control of hadrontherapy. Note that such PG monitoring is also considered in the case of boron neutron capture therapy (see *e.g.* [152]), or in proton boron fusion therapy. The latter is based on the capture by ^{11}B leading to 3 α particles [153]. Petringa et al. have studied the possibility to monitor treatments with ^{10}B and ^{11}B by means of PG [154]. Indeed, the adjunction of ^{10}B enhances the yields of several lines in the range 0.4–1.4 MeV. Also, the PG imaging systems, especially 3D-imaging (Compton cameras) may have applications, in more general SPECT medical imaging, opening the possibility to use higher-energy gamma imaging than currently used.

5. Discussion in view of clinical applicability

5.1. Beam time structure

A very important feature for the detection of PGs is the beam time structure, depending on the type of accelerator and on the ion species. Table 3 gives some typical time structures of various clinical accelerator types.

Cyclotrons are widely used for proton therapy. They deliver fixed-energy particles with short nano-bunches (a fraction of nanosecond to a few nanoseconds) at about 100 MHz frequency, and energy variations for PBS are made by means of passive degraders with a target and energy spread selection inside a spectrometer located at the exit of the cyclotron. Therefore, the bunch time-width at the isocenter of the treatment room is mainly dominated by the beam momentum spread. The duty cycle is typically 10%. At nA current operation, the number of protons per bunch is about 10^2. Thus synchronization of PG detection with the beam HF provides substantial reduction of the background. However, each time the energy is varied, re-synchronization is necessary.

Synchrotrons are, until now, the only accelerators used for therapy with ions heavier than protons. They are also used for proton therapy. The beam time structure is characterized by a macro-structure (1–10 s period) corresponding to the cycle of injection-acceleration-extraction. The energy may be varied between two cycles. The extracted beam has in addition a sub-structure with 20–40 ns bunches every 100–200 ns (for carbon synchrotrons like HIT-Heidelberg, and $\approx$ 3–5 times smaller for proton synchrotrons), related to the spatial extension and revolution period of ion bunches inside the accelerator ring. The overall duty factor of such accelerators is also of the order of 10%, and the number of protons per bunch is also about 10^2 in the case of protons, and a few units for carbon-ion beams. TOF may become poorly efficient for PG detection in proton therapy with synchrotrons, since it will not enable one to suppress neutron-induced background during bunches exceeding 5–10 ns [85]. For carbon-ion therapy, the detection of individual ion impacts, although challenging, is doable at mean intensities of $10^7 - 10^8$ ions/s, by means of fast beam hodoscopes.

A new generation of superconducting *synchrocyclotrons* (IBA, Mevion) is emerging. Such accelerators combine nanostructures with bunches of a few ns duration and variable period ($\simeq$10–15 ns), and micro-structures with 1 ms cycle and 7 μs extraction duration (IBA-S2C2). Thus the overall duty cycle of such accelerators is close to 1/1000, and a very high number of protons per nanobunch ($\approx 10^4$). The long pause periods between micro-bunches provides new interest for in-beam PET. The efficiency of TOF-PG detection will be conditioned by an adequate synchronization with the beam nanopulses, which may also require the use of a fast beam monitor since the frequency varies during extraction. The three examples presented here show that PG detection systems may be different depending of the type of accelerator.

5.2. Ion species

Carbon ion beams are more subject to fragmentation than proton ones. As a first consequence PG yields are higher for carbon ions than for protons, typically by a factor 5–6. As second consequence, light fragments issued from carbon-ion beams, like protons and neutrons, also create fragmentation vertices out of the primary ion path. As illustrated in Fig. 2, for 310 MeV/u carbon ions incident in water, PG induced by secondaries are rapidly more numerous than primary ones as the penetration depth increases, and the contrast at the range-end falloff is much less pronounced than in the case of protons. In addition, these secondaries are themselves a source of background in PG detection, for which discrimination strategies like TOF are necessary for carbon ions. As written above, carbon ions produce more PGs than protons per projectile. However, much less carbon ions are necessary to deposit the same amount of physical dose, due to the Z^2 dependence of LET (Linear Energy Transfer). Taking into account the higher carbon RBE in the SOBP region, typically 10^2 times more protons than carbon ions are necessary to irradiate a given tumor volume at the same therapeutical dose. *In fine*, the number of PG with proton beams is $\simeq$ 20 times larger than for carbon-ion beams, with less background and better contrast to noise at the Bragg-peak falloff. Therefore, it is unrealistic to achieve online verification of carbon-ion range with millimetric precision at the pencil beam scale, with the gamma cameras that are under development. Efficiencies of the order of 10^{-2} would be necessary, which corresponds to the spatial coverage of PET ring devices. Nevertheless, *a posteriori* verification of a treatment fraction in carbon-ion therapy is still possible, like for PET. So far no comparison between PET and PGI performances has been performed for carbon-ion therapy.

Table 3
Typical time structures of various clinical accelerator types.

		Synchrotron		Cyclotron (IBA, Varian)	Synchro-cyclotron (S2C2, IBA)
		Carbon	Protons		
Typical intensity (ions/s)		10^7	10^9	10^{10}	$\sim 10^{10}$
Macrostructure	Period (s)	1–10		∅	10^{-3}
	Bunch width (ns)	20–50		0.5–2	8
Microstructure	Period (ns)	100–200		10	16 (variable)
	Ions/bunch	2–5		200	4000

5.3. PG vs other modalities

In-beam PET imaging: As PET imaging consists in the detection of two coincident photons, either dual head detection systems are employed [155–157], or more sophisticated geometries like deformable or cylindric-with-hole ring configurations are proposed [158,159]. The most abundant β^+ emitters like ^{15}O or ^{11}C have lifetimes of several minutes (122 s and 20.4 min respectively), and therefore the acquisition of sufficient statistics requires one to several minutes of data acquisition [14], which makes it profitable for an *a posteriori* control. Indeed, the accumulation of statistics during such a long time corresponds to the contribution of many beam spots, at several energies. Improving solutions for in-beam PET has been one of the goals of the recent ENVISION FP7 project, and is still under investigation by many groups. Recently, Dendooven et al. proposed to make measurements during beam delivery of very short lifetime emitters like ^{12}N (11 ms) that are produced during collisions of protons on carbon nuclei [160]. This may open the way to near real-time imaging, provided fast reconstruction, and signal-to-noise discrimination issues are solved. More generally, the latter point must be addressed via very fast timing, which is one of the main challenges in PET imaging at the moment.

Moteabbed et al. [29] performed a comparison between PET and PG range verifications in proton therapy by means of simulations with GEANT4.9.0 for several clinical cases, and for both passive and active beam delivery modes. With this version of the simulation toolkit (which overestimated PG yields, see Section 2), PG production yields were typically 10 times higher than β^+ disintegration ones, and the average transmission of the 2–8 MeV PG photons through the patient is 4–5.5 times larger than for 511 keV ones. Washout was taken into account, but only as a reduction of the β^+ disintegration yield due to the time-delay for transportation (2 min after stopping the irradiation) to an in-room PET-imaging device, and to an acquisition time duration of 5 min, and thus no metabolic spread of the radionuclides was considered. The statistics reduction due to washout is typically by a factor 1/6 to 1/7. As in-room PET scanners have a much larger efficiency ($\epsilon \approx 2 \times 10^{-2}$) than PGI prototypes ($\epsilon < 10^{-3}$), PET images still remained with higher statistics. One of their conclusions was that the PG method could be advantageous during active pencil beam scanning, especially for smaller tumors located in heterogeneous anatomical locations. Note also that, in proton therapy, 1D-PET falloffs are located 5–6 mm proximal to the PG falloffs, that are much closer to the dose falloff [29]. As for carbon-ion therapy, enhanced contrast at the Bragg peak region comes for projectile-like radioisotopes ^{10}C and ^{11}C.

Proton vertex imaging: secondary proton yields are not relevant for proton beams since they are unlikely to escape the patient, but they are of the order of 3 per incident carbon ion. Only few of them will emerge from the patient at measurable energy (see Fig. 1), but they will be quite forward peaked and easy to detect by tracking devices. Despite the fact that high energy secondary protons are more likely emitted from vertices far upstream of the Bragg peak, where carbon primaries still have the highest energy, the reconstructed vertex distribution is connected with the ion range [17,16]. Small size pixelated detectors could be used, or large acceptance ones, which could enable observations at large angles [161–163]. However, further studies are needed to qualify the method in the case of heterogeneous targets [164,165].

5.4. Statistics issue

Regardless of the method used to monitor the range of the primary beam during therapy, the main issue is the available statistics to optimize the information. This has been studied in details for PGI [89,32], but also for secondary proton vertex imaging [16] and PET.

According to Eq. (1), the falloff retrieval precision (FRP) – or equivalently the rise at the patient entrance – is inversely proportional to the signal-to-noise ratio, and therefore scales like the inverse square root of the statistics. Improving the spatial resolution of an imaging device (in the sense of decreasing the width of the point spread function response) will be done at the expense of the statistics per spatial unit, and thus should result from a compromise between FRP and the complexity of the distribution at emission. The latter is important in the case of mixed beams traversing a heterogeneous medium, thus for protons rather than carbon ion beams [166].

The most efficient way to increase the available statistics is to accumulate the information from several beam spots, when they correspond to the same expected range, but this will be done at the expense of some loss in transverse spatial information, and possible blurring if heterogeneities enter into play.

6. Clinical status, remaining challenges, perspectives and conclusion

The first clinical verifications of proton ranges with patients have been performed with the IBA-knife-edge camera prototype. First at Oncoray-Dresden with passive beam delivery [97], and, more recently, with PBS at Philadelphia [98], where two patients were followed, and range deviations were measured using grouping of iso-energy spots. The precision on the range deviations is better than the uncertainty margins.

PG verification of treatments is based on comparisons between measured data and predicted ones, according to the treatment plans. Therefore, simulations should be reliable enough to provide predictions with a precision at the level of the deviations to be detected. At the moment, it seems that the ICRU 63 experimental database is sufficient to perform reliable predictions for imaging systems like the IBA prototype [43,98]. However non-imaging system (e.g. PGS that derives ion-range estimate from PG energy) may require more precise experimental data or nuclear models. Hence improving cross section data bases, as a function of materials, ion species and energy, is still necessary. Besides it is worth noting that background simulation is problematic for two reasons: it requires the modeling of interactions (mainly neutrons) in the full treatment room leading to prohibitive computing times and the background predictions (based on experimental database or nuclear models) are not satisfying. In practice, the background is therefore not modeled and it is taken into account in the IBA prototype prediction tool by adding an offset to the fitting procedure of the measured PG profiles [43].

To go beyond PG range verification *i.e.* toward dose verification an inverse problem solving based on the 3D prompt-gamma distribution is necessary. In intensity modulated RT online 3D-dose verification has now been developed, usually based on the 2D fluence modeling with arrays of ionization chambers or EPID detectors [167]. To translate such patient-specific QA protocol to hadrontherapy only a few approaches have yet been proposed, such as the filtering-based approach from Schumann et al. [55] which was inspired by previous works in PET [51,168].

The address of inhomogeneous region in the patient will definitively need express care.

One may also consider the concept of multimodal detection systems, coupling for instance integrated measurements like PGT or PGPI with PG imaging, or PG and PET detection. A PET-PGI system could be achieved with several Compton cameras as an hybrid detection system, as foreseen by the Munich group [169]. The INSIDE multi-modal project, coupling PET and IVI for carbon ion beams [156,170] is being implemented at CNAO. PET devices could also be used standalone, but with dual trigger system, in order to detect PGs in integration mode during beam delivery, and PET coincidences during beam pauses.

Further improvement of the PGT, PGPI, but also PGI using TOF, will be obtained by using very fast timing. This challenge concerns the gamma detection by itself, but also the beam triggering, for which ultra-fast, large-area diamond detectors could serve as a radiation-hard, 2D beam hodoscope [171].

The clinical implementation of PG monitoring devices will depend on the type of accelerator and the beam delivery mode. We have seen that for some of the devices like Compton cameras, but also more conventional cameras with limited acquisition rates, reduced intensities could be necessary during the very first distal spots. The time needed to control the position of such spots could be quite small, of the order of a second, before the treatment resumes at nominal intensity if the green light is obtained. Thus, beam delivery protocols could be modified in order to include the feedback of the PG signal.

The work presented here represents nearly 15 years of progress between the first idea, and the present ongoing clinical trials involving prompt-gamma prototypes. This period has been rich with emerging new ideas and concepts, which were also accompanied by significant progress in other modalities for online in vivo monitoring of hadron-therapy.

In Europe in particular, FP7 projects such as ENVISION, ENTER-VISION and ULICE, coordinated within the Enlight framework, were very helpful to structure collaborations. Presently the Medinet Network helps such a structuration. The authors would also like to acknowledge France Hadron (ANR-11-INBS-0007), and the LABEX PRIMES (ANR-11-LABX-0063). Katia Parodi is warmly thanked by the authors for a careful reading and suggestions for improving the quality of the manuscript.

References

[1] D. Schardt, T. Elsässer, D. Schulz-Ertner, Heavy-ion tumor therapy: Physical and radiobiological benefits, Rev. Modern Phys. 82 (1) (2010) 383. http://dx.doi.org/10.1103/RevModPhys.82.383.

[2] M. Durante, D.J. Brenner, S.C. Formenti, Does heavy ion therapy work through the immune system? Int. J. Radiat. Oncol. Biol. Phys. 96 (5) (2016) 934–936. http://dx.doi.org/10.1016/j.ijrobp.2016.08.037.

[3] W.D. Newhauser, R. Zhang, The physics of proton therapy, Phys. Med. Biol. 60 (8) (2015) R155–R209. http://dx.doi.org/10.1088/0031-9155/60/8/r155.

[4] J. Remillieux, J.-M. Moreau, D. Dauvergne, J. Balosso, Les enjeux de l'hadronthérapie par ions carbone, Reflets Phys. 43 (2015) 26–30. http://dx.doi.org/10.1051/refdp/201543026. http://www.refletsdelaphysique.fr/10.1051/refdp/201543026.

[5] U. Amaldi, G. Magrin, Accelerators in medicine, in: S. Myers, H. Schopper (Eds.), Accelerators and Colliders, in: Landolt–Börnstein — Group I Elementary Particles, Nuclei and Atoms, Springer, Berlin, Heidelberg, 2013, pp. 488–513.

[6] M. Cunha, C. Monini, E. Testa, M. Beuve, NanOx, a new model to predict cell survival in the context of particle therapy, Phys. Med. Biol. 62 (2017) 1248–1268. http://dx.doi.org/10.1088/1361-6560/aa54c9.

[7] A.-C. Knopf, A. Lomax, In vivo proton range verification: a review, Phys. Med. Biol. 58 (15) (2013) R131–160. http://dx.doi.org/10.1088/0031-9155/58/15/R131.

[8] H. Paganetti, Range uncertainties in proton therapy and the role of Monte Carlo simulations, Phys. Med. Biol. 57 (11) (2012) R99–R117. http://dx.doi.org/10.1088/0031-9155/57/11/R99.

[9] W. Assmann, S. Kellnberger, S. Reinhardt, S. Lehrack, A. Edlich, P.G. Thirolf, M. Moser, G. Dollinger, M. Omar, V. Ntziachristos, K. Parodi, Ionoacoustic characterization of the proton Bragg peak with submillimeter accuracy, Med. Phys. 42 (2) (2015) 567–574. http://dx.doi.org/10.1118/1.4905047.

[10] M. Yamaguchi, Y. Nagao, K. Ando, S. Yamamoto, T. Toshito, J. Kataoka, N. Kawachi, Secondary-electron-bremsstrahlung imaging for proton therapy, Nucl. Instrum. Methods Phys. Res. A 833 (0) (2016) 199–207. http://dx.doi.org/10.1016/j.nima.2016.07.034.

[11] M.F. Gensheimer, T.I. Yock, N.J. Liebsch, G.C. Sharp, H. Paganetti, N. Madan, P.E. Grant, T. Bortfeld, In vivo proton beam range verification using spine MRI changes, Int. J. Radiat. Oncol. Biol. Phys. 78 (1) (2010) 268–275. http://dx.doi.org/10.1016/j.ijrobp.2009.11.060.

[12] B.M. Oborn, S. Dowdell, P.E. Metcalfe, S. Crozier, R. Mohan, P.J. Keall, Proton beam deflection in MRI fields: Implications for MRI-guided proton therapy, Med. Phys. 42 (5) (2015) 2113–2124. http://dx.doi.org/10.1118/1.4916661. 00002.

[13] W. Enghardt, K. Parodi, P. Crespo, F. Fiedler, J. Pawelke, F. Pönisch, Dose quantification from in-beam positron emission tomography, Radiother. Oncol. 73 (2004) S96–S98. http://dx.doi.org/10.1016/S0167-8140(04)80024-0.

[14] M.G. Bisogni, A. Attili, G. Battistoni, N. Belcari, N. Camarlinghi, P. Cerello, S. Coli, A. Del Guerra, A. Ferrari, V. Ferrero, E. Fiorina, G. Giraudo, E. Kostara, M. Morrocchi, F. Pennazio, C. Peroni, M.A. Piliero, G. Pirrone, A. Rivetti, M.D. Rolo, V. Rosso, P. Sala, G. Sportelli, R. Wheadon, INSIDE in-beam positron emission tomography system for particle range monitoring in hadrontherapy, Journal of Medical Imaging 4 (1) (2016) 011005. http://dx.doi.org/10.1117/1.JMI.4.1.011005.

[15] U. Amaldi, R. Bonomi, S. Braccini, M. Crescenti, A. Degiovanni, M. Garlasché, A. Garonna, G. Magrin, C. Mellace, P. Pearce, G. Pittà, P. Puggioni, E. Rosso, S. Verdú Andrés, R. Wegner, M. Weiss, R. Zennaro, Accelerators for hadrontherapy: From Lawrence cyclotrons to linacs, Nucl. Instrum. Methods Phys. Res. A 620 (2–3) (2010) 563–577. http://dx.doi.org/10.1016/j.nima.2010.03.130.

[16] P. Henriquet, E. Testa, M. Chevallier, D. Dauvergne, G. Dedes, N. Freud, J. Krimmer, J.M. Létang, C. Ray, M.-H. Richard, F. Sauli, Interaction vertex imaging (IVI) for carbon ion therapy monitoring: a feasibility study, Phys. Med. Biol. 57 (14) (2012) 4655. http://dx.doi.org/10.1088/0031-9155/57/14/4655.

[17] K. Gwosch, B. Hartmann, J. Jakubek, C. Granja, P. Soukup, O. Jäkel, M. Martišíková, Non-invasive monitoring of therapeutic carbon ion beams in a homogeneous phantom by tracking of secondary ions, Phys. Med. Biol. 58 (11) (2013) 3755. http://dx.doi.org/10.1088/0031-9155/58/11/3755.

[18] F. Stichelbaut, Y. Jongen, Verification of the proton beams position in the patient by the detection of prompt gamma-rays emission, in: 39th Meeting of the Particle Therapy Co-Operative Group, San Francisco, CA, October 2003, 2003.

[19] C.-H. Min, C.H. Kim, M.-Y. Youn, J.-W. Kim, Prompt gamma measurements for locating the dose falloff region in the proton therapy, Appl. Phys. Lett. 89 (18) (2006) 183517. http://dx.doi.org/10.1063/1.2378561.

[20] E. Testa, M. Bajard, M. Chevallier, D. Dauvergne, F.L. Foulher, N. Freud, J.-M. Letang, J.-C. Poizat, C. Ray, M. Testa, Monitoring the Bragg peak location of 73 MeV/u carbon ions by means of prompt gamma-ray measurements, Appl. Phys. Lett. 93 (9) (2008) 093506. http://dx.doi.org/10.1063/1.2975841.

[21] J.M. Verburg, J. Seco, Proton range verification through prompt gamma-ray spectroscopy, Phys. Med. Biol. 59 (23) (2014) 7089. http://dx.doi.org/10.1088/0031-9155/59/23/7089.

[22] C. Golnik, F. Hueso-González, A. Müller, P. Dendooven, W. Enghardt, F. Fiedler, T. Kormoll, K. Roemer, J. Petzoldt, A. Wagner, G. Pausch, Range assessment in particle therapy based on prompt gamma-ray timing measurements, Phys. Med. Biol. 59 (18) (2014) 5399. http://dx.doi.org/10.1088/0031-9155/59/18/5399.

[23] J. Krimmer, G. Angellier, L. Balleyguier, D. Dauvergne, N. Freud, J. Hérault, J. Létang, H. Mathez, M. Pinto, E. Testa, Y. Zoccarato, A cost-effective monitoring technique in particle therapy via uncollimated prompt gamma peak integration, Appl. Phys. Lett. 110 (15) (2017) 154102. http://dx.doi.org/10.1063/1.4980103.

[24] M. Pinto, M. Bajard, S. Brons, M. Chevallier, D. Dauvergne, G. Dedes, M. De Rydt, N. Freud, J. Krimmer, C. La Tessa, J.M. Létang, K. Parodi, R, R. Pleskač, D. Prieels, C. Ray, I. Rinaldi, F. Roellinghoff, D. Schardt, E. Testa, M. Testa, Absolute prompt-gamma yield measurements for ion beam therapy monitoring, Phys. Med. Biol. 60 (2) (2015) 565. http://dx.doi.org/10.1088/0031-9155/60/2/565.

[25] M. Pinto, D. Dauvergne, N. Freud, J. Krimmer, J.M. Létang, E. Testa, Assessment of Geant4 prompt-gamma emission yields in the context of proton therapy monitoring, Front. Oncol. (2016) 10. http://dx.doi.org/10.3389/fonc.2016.00010.

[26] C. Robert, G. Dedes, G. Battistoni, T.T. Böhlen, I. Buvat, F. Cerutti, M.P.W. Chin, A. Ferrari, P. Gueth, C. Kurz, L. Lestand, A. Mairani, G. Montarou, R. Nicolini, P.G. Ortega, K. Parodi, Y. Prezado, P.R. Sala, D. Sarrut, E. Testa, Distributions of secondary particles in proton and carbon-ion therapy: a comparison between GATE/Geant4 and FLUKA Monte Carlo codes, Phys. Med. Biol. 58 (9) (2013) 2879–2899. http://dx.doi.org/10.1088/0031-9155/58/9/2879.

[27] K. Gunzert-Marx, H. Iwase, D. Schardt, R.S. Simon, Secondary beam fragments produced by 200 MeV/u ^{12}C ions in water and their dose contributions in carbon ion radiotherapy, New J. Phys. 10 (7) (2008) 075003. http://dx.doi.org/10.1088/1367-2630/10/7/075003.

[28] V. Reithinger, Assurance qualité des traitements par hadronthérapie carbone par imagerie de particules promptes chargées, Université Claude Bernard - Lyon I, 2015 (Ph.D. thesis). https://tel.archives-ouvertes.fr/tel-01441452/document.

[29] M. Moteabbed, S. España, H. Paganetti, Monte Carlo patient study on the comparison of prompt gamma and PET imaging for range verification in proton therapy, Phys. Med. Biol. 56 (2011) 1063–1082. http://dx.doi.org/10.1088/0031-9155/56/4/012.

[30] L. Grevillot, D. Bertrand, F. Dessy, N. Freud, D. Sarrut, GATE as a GEANT4-based Monte Carlo platform for the evaluation of proton pencil beam scanning treatment plans., Phys. Med. Biol. 57 (13) (2012) 4223–4244. http://dx.doi.org/10.1088/0031-9155/57/13/4223.

[31] M. Krämer, O. Jäkel, T. Haberer, G. Kraft, D. Schardt, U. Weber, Treatment planning for heavy-ion radiotherapy: physical beam model and dose optimization, Phys. Med. Biol. 45 (11) (2000) 3299. http://dx.doi.org/10.1088/0031-9155/45/11/313.

[32] F. Roellinghoff, A. Benilov, D. Dauvergne, G. Dedes, N. Freud, G. Janssens, J. Krimmer, J.M. Létang, M. Pinto, D. Prieels, C. Ray, J. Smeets, F. Stichelbaut, E. Testa, Real-time proton beam range monitoring by means of prompt-gamma detection with a collimated camera, Phys. Med. Biol. 59 (5) (2014) 1327. http://dx.doi.org/10.1088/0031-9155/59/5/1327.

[33] G. Dedes, K. Parodi, Monte Carlo simulations of particle interactions with tissue in carbon ion therapy, Int. J. Particle Therapy 2 (3) (2015) 447–458. http://dx.doi.org/10.14338/ijpt-15-00021.

[34] A. Schumann, J. Petzoldt, P. Dendooven, W. Enghardt, C. Golnik, F. Hueso-González, T. Kormoll, G. Pausch, K. Roemer, F. Fiedler, Simulation and experimental verification of prompt gamma-ray emissions during proton irradiation, Phys. Med. Biol. 60 (10) (2015) 4197. http://dx.doi.org/10.1088/0031-9155/60/10/4197.

[35] N. Qin, M. Pinto, Z. Tian, G. Dedes, A. Pompos, S.B. Jiang, K. Parodi, J. X, Initial development of goCMC: a GPU-oriented fast cross-platform Monte Carlo engine for carbon ion therapy., Phys. Med. Biol. 62 (2017) 3682–3699. http://dx.doi.org/10.1088/1361-6560/aa5d43.

[36] D. Giantsoudi, J. Schuemann, X. Jia, S. Dowdell, S. Jiang, H. Paganetti, Validation of a GPU-based Monte Carlo code (gPMC) for proton radiation therapy: clinical cases study, Phys. Med. Biol. 60 (6) (2015) 2257–2269. http://dx.doi.org/10.1088/0031-9155/60/6/2257.

[37] J. Seco, F. Verhaegen, Monte Carlo Techniques in Radiation Therapy, first ed. in: Imaging in Medical Diagnosis and Therapy, CRC Press, 2013.

[38] F. Sommerer, F. Cerutti, K. Parodi, A. Ferrari, W. Enghardt, H. Aiginger, In-beam PET monitoring of mono-energetic ^{16}O and ^{12}C beams: experiments and FLUKA simulations for homogeneous targets, Phys. Med. Biol. 54 (13) (2009) 3979–3996. http://dx.doi.org/10.1088/0031-9155/54/13/003.

[39] D. Sarrut, M. Bardiès, N. Boussion, N. Freud, S. Jan, J.-M. Létang, G. Loudos, L. Maigne, S. Marcatili, T. Mauxion, et al., A review of the use and potential of the GATE Monte Carlo simulation code for radiation therapy and dosimetry applications, Med. Phys. 41 (6) (2014) 064301. http://dx.doi.org/10.1118/1.4871617.

[40] K. Parodi, A. Ferrari, F. Sommerer, H. Paganetti, Clinical CT-based calculations of dose and positron emitter distributions in proton therapy using the FLUKA Monte Carlo code, Phys. Med. Biol. 52 (12) (2007) 3369–3387. http://dx.doi.org/10.1088/0031-9155/52/12/004.

[41] W. El Kanawati, J.M. Létang, D. Dauvergne, M. Pinto, D. Sarrut, E. Testa, N. Freud, Monte Carlo simulation of prompt γ-ray emission in proton therapy using a specific track length estimator, Phys. Med. Biol. 60 (20) (2015) 8067–8086. http://dx.doi.org/10.1088/0031-9155/60/20/8067.

[42] B.F.B. Huisman, J.M. Létang, É. Testa, D. Sarrut, Accelerated prompt gamma estimation for clinical proton therapy simulations, Phys. Med. Biol. 61 (21) (2016) 7725–7743. http://dx.doi.org/10.1088/0031-9155/61/21/7725.

[43] E. Sterpin, G. Janssens, J. Smeets, F.V. Stappen, D. Prieels, M. Priegnitz, I. Perali, S. Vynckier, Analytical computation of prompt gamma ray emission and detection for proton range verification, Phys. Med. Biol. 60 (12) (2015) 4915. http://dx.doi.org/10.1088/0031-9155/60/12/4915.

[44] G. Russo, A. Attili, G. Battistoni, D. Bertrand, F. Bourhaleb, F. Cappucci, M. Ciocca, A. Mairani, F.M. Milian, S. Molinelli, M.C. Morone, S. Muraro, T. Orts, V. Patera, P. Sala, E. Schmitt, G. Vivaldo, F. Marchetto, A novel algorithm for the calculation of physical and biological irradiation quantities in scanned ion beam therapy: the beamlet superposition approach, Phys. Med. Biol. 61 (1) (2016) 183–214. http://dx.doi.org/10.1088/0031-9155/61/1/183.

[45] ICRU, Report No. 63: Nuclear data for beutron and proton radiotherapy and for radiation protection, Tech. Rep. 5, in: Medical Physics, 28, Wiley-Blackwel, International Commission in Radiation Units & Measurements, 2001, p. 861. http://dx.doi.org/10.1118/1.1369116.

[46] S. Helmbrecht, M. Priegnitz, W. Enghardt, H. Rohling, F. Fiedler, Application of a yield approach for the prediction of positron emitter distributions produced during therapeutic carbon-ion beam irradiation, IEEE Trans. Nucl. Sci. 63 (1) (2016) 61–69. http://dx.doi.org/10.1109/TNS.2015.2481489.

[47] A. Miyatake, T. Nishio, T. Ogino, Development of activity pencil beam algorithm using measured distribution data of positron emitter nuclei generated by proton irradiation of targets containing ^{12}C, ^{16}O, and ^{40}Ca nuclei in preparation of clinical application, Med. Phys. 38 (10) (2011) 5818–5829. http://dx.doi.org/10.1118/1.3641829.

[48] H.W. De Jong, E.T. Slijpen, F.J. Beekman, Acceleration of Monte Carlo SPECT simulation using convolution-based forced detection, IEEE Trans. Nucl. Sci. 48 (1) (2001) 58–64. http://dx.doi.org/10.1109/23.910833.

[49] P. Descourt, T. Carlier, Y. Du, X. Song, I. Buvat, E. Frey, M. Bardies, B. Tsui, D. Visvikis, Implementation of angular response function modeling in SPECT simulations with GATE, Phys. Med. Biol. 55 (9) (2010) N253. http://dx.doi.org/10.1088/0031-9155/55/9/N04.

[50] K. Kroniger, M. Herzog, G. Landry, E. Traneus, G. Dedes, K. Parodi, A fast analytical approach for prompt gamma and PET predictions in a TPS for proton range verification, Med. Phys. 42 (6) (2015) 3199. http://dx.doi.org/10.1118/1.4923825.

[51] K. Parodi, T. Bortfeld, A filtering approach based on Gaussian-powerlaw convolutions for local PET verification of proton radiotherapy, Phys. Med. Biol. 51 (8) (2006) 1991–2009. http://dx.doi.org/10.1088/0031-9155/51/8/003.

[52] F. Attanasi, A. Knopf, K. Parodi, H. Paganetti, T. Bortfeld, V. Rosso, A. Del Guerra, Extension and validation of an analytical model for in vivo PET verification of proton therapy — a phantom and clinical study, Phys. Med. Biol. 56 (16) (2011) 5079. http://dx.doi.org/10.1088/0031-9155/56/16/001.

[53] K. Frey, J. Bauer, D. Unholtz, C. Kurz, M. Krämer, T. Bortfeld, K. Parodi, TPS(PET) — a TPS-based approach for in vivo dose verification with PET in proton therapy, Phys. Med. Biol. 59 (1) (2014) 1–21. http://dx.doi.org/10.1088/0031-9155/59/1/1.

[54] L. Grevillot, D. Bertrand, F. Dessy, N. Freud, D. Sarrut, A Monte Carlo pencil beam scanning model for proton treatment plan simulation using GATE/GEANT4, Phys. Med. Biol. 56 (16) (2011) 5203. http://dx.doi.org/10.1088/0031-9155/56/16/008.

[55] A. Schumann, M. Priegnitz, S. Schoene, W. Enghardt, H. Rohling, F. Fiedler, From prompt gamma distribution to dose: a novel approach combining an evolutionary algorithm and filtering based on Gaussian-powerlaw convolutions, Phys. Med. Biol. 61 (19) (2016) 6919. http://dx.doi.org/10.1088/0031-9155/61/19/6919.

[56] T.T. Böhlen, F. Cerutti, M. Dosanjh, A. Ferrari, I. Gudowska, A. Mairani, J.M. Quesada, Benchmarking nuclear models of FLUKA and GEANT4 for carbon ion therapy, Phys. Med. Biol. 55 (19) (2010) 5833–5847. http://dx.doi.org/10.1088/0031-9155/55/19/014. PMID: 20844337.

[57] J.M. Verburg, H.A. Shih, J. Seco, Simulation of prompt gamma-ray emission during proton radiotherapy, Phys. Med. Biol. 57 (17) (2012) 5459. http://dx.doi.org/10.1088/0031-9155/57/17/5459.

[58] J. Ready, Development of a multi-knife-edge slit collimator for prompt gamma ray imaging during proton beam cancer therapy, UC Berkeley, 2016 (Ph.D. thesis), http://escholarship.org/uc/item/14d0r6zb.

[59] G. Dedes, M. Pinto, D. Dauvergne, N. Freud, J. Krimmer, J.M. Létang, C. Ray, E. Testa, Assessment and improvements of Geant4 hadronic models in the context of prompt-gamma hadrontherapy monitoring, Phys. Med. Biol. 59 (7) (2014) 1747. http://dx.doi.org/10.1088/0031-9155/59/7/1747.

[60] L. Kelleter, A. Wrońska, J. Besuglow, A. Konefał, K. Laihem, J. Leidner, A. Magiera, K. Parodi, K. Rusiecka, A. Stahl, T. Tessonnier, Spectroscopic study of prompt-gamma emission for range verification in proton therapy, Phys. Med. 34 (2017) 7–17. http://dx.doi.org/10.1016/j.ejmp.2017.01.003.

[61] J. Krimmer, M. Chevallier, J. Constanzo, D. Dauvergne, M. De Rydt, G. Dedes, N. Freud, P. Henriquet, C. La Tessa, J. Létang, R. Pleskaè, M. Pinto, C. Ray, V. Reithinger, M. Richard, I. Rinaldi, F. Roellinghoff, C. Schuy, E. Testa, M. Testa, Collimated prompt gamma TOF measurements with multi-slit multi-detector configurations, J. Instrum. 10 (01) (2015) P01011. http://dx.doi.org/10.1088/1748-0221/10/01/P01011.

[62] D. Dauvergne, J. Krimmer, V. Reithinger, E. Testa, A beam monitor for Time of Flight measurement of prompt radiations, Tech. Rep. ENVISION Report D3.5, CNRS, 2014.

[63] J. Krimmer, L. Caponetto, X. Chen, M. Chevallier, D. Dauvergne, M. De Rydt, G. Dedes, S.M. Deng, J.-L. Ley, H. Mathez, C. Ray, V. Reithinger, E. Testa, Y. Zoccarato, Real-time monitoring of the ion range during hadrontherapy: An update on the beam tagging hodoscope, Radiother. Oncol. 110 (1) (2014) S54. http://dx.doi.org/10.1016/S0167-8140(15)34132-3.

[64] Y. Mizumura, T. Tanimori, H. Kubo, A. Takada, J.D. Parker, T. Mizumoto, S. Sonoda, D. Tomono, T. Sawano, K. Nakamura, Y. Matsuoka, S. Komura, S. Nakamura, M. Oda, K. Miuchi, S. Kabuki, Y. Kishimoto, S. Kurosawa, S. Iwaki, Development of a 30 cm-cube electron-tracking Compton camera for the SMILE-II experiment, J. Instrum. 9 (05) (2014) C05045. http://dx.doi.org/10.1088/1748-0221/9/05/c05045.

[65] X. Lojacono, M.-H. Richard, J.-L. Ley, E. Testa, C. Ray, N. Freud, J. Létang, D. Dauvergne, V. Maxim, R. Prost, Low statistics reconstruction of the Compton camera point spread function in 3D prompt-gamma Imaging of ion beam therapy, IEEE Trans. Nucl. Sci. 60 (5) (2013) 3355–3363. http://dx.doi.org/10.1109/TNS.2013.2275200.

[66] V. Maxim, Filtered backprojection reconstruction and redundancy in Compton camera imaging, IEEE Trans. Image Process. 23 (1) (2014) 332–341. http://dx.doi.org/10.1109/TIP.2013.2288143.

[67] V. Maxim, X. Lojacono, E. Hilaire, J. Krimmer, E. Testa, D. Dauvergne, I. Magnin, R. Prost, Probabilistic models and numerical calculation of system matrix and sensitivity in list-mode MLEM 3D reconstruction of Compton camera images, Phys. Med. Biol. 61 (1) (2016) 243. http://dx.doi.org/10.1088/0031-9155/61/1/243.

[68] S. Schoene, W. Enghardt, F. Fiedler, C. Golnik, G. Pausch, H. Rohling, T. Kormoll, An image reconstruction framework and camera prototype aimed for compton imaging for *in-vivo* dosimetry of therapeutic ion beams, IEEE Trans. Radiat. Plasma Med. Sci. 1 (1) (2017) 96–107. http://dx.doi.org/10.1109/tns.2016.2623220.

[69] D. Mackin, S. Peterson, S. Beddar, J. Polf, Evaluation of a stochastic reconstruction algorithm for use in Compton camera imaging and beam range verification from secondary gamma emission during proton therapy, Phys. Med. Biol. 57 (11) (2012) 3537. http://dx.doi.org/10.1088/0031-9155/57/11/3537.

[70] J.C. Polf, S. Avery, D.S. Mackin, S. Beddar, Imaging of prompt gamma rays emitted during delivery of clinical proton beams with a Compton camera: feasibility studies

for range verification, Phys. Med. Biol. 60 (18) (2015) 7085. http://dx.doi.org/10.1088/0031-9155/60/18/7085.

[71] A. Andreyev, A. Celler, I. Ozsahin, A. Sitek, Resolution recovery for Compton camera using origin ensemble algorithm, Med. Phys. 43 (2016) 4866. http://dx.doi.org/10.1118/1.4959551.

[72] J.E. Gillam, C. Lacasta, I. Torres-Espallardo, C. Candela Juan, G. Llosá, P. Solevi, J. Barrio, M. Rafecas, A Compton imaging algorithm for on-line monitoring in hadron therapy, Proc. SPIE Med. Imaging 7961 (2011) 796110. http://dx.doi.org/10.1117/12.877678.

[73] P.G. Ortega, I. Torres-Espallardo, F. Cerutti, A. Ferrari, J.E. Gillam, C. Lacasta, G. Llosá, J.F. Oliver, P.R. Sala, P. Solevi, M. Rafecas, Noise evaluation of Compton camera imaging for proton therapy, Phys. Med. Biol. 60 (5) (2015) 1845. http://dx.doi.org/10.1088/0031-9155/60/5/1845.

[74] M.C. Hamel, J.K. Polack, A. Poitrasson-Rivière, S.D. Clarke, S.A. Pozzi, Localization and spectral isolation of special nuclear material using stochastic image reconstruction, Nucl. Instrum. Methods Phys. Res. A 841 (2017) 24–33. http://dx.doi.org/10.1016/j.nima.2016.10.004.

[75] J. Kiener, M. Berheide, N.L. Achouri, A. Boughrara, A. Coc, A. Lefebvre, F. de Oliveira Santos, C. Vieu, γ–ray production by inelastic proton scattering on 16O and 12C, Phys. Rev. C 58 (4) (1998) 2174–2179. http://dx.doi.org/10.1103/PhysRevC.58.2174.

[76] P. Dyer, D. Bodansky, A.G. Seamster, E.B. Norman, D.R. Maxson, Cross sections relevant to gamma-ray astronomy: Proton induced reactions, Phys. Rev. C 23 (1981) 1865–1882. http://dx.doi.org/10.1103/PhysRevC.23.1865.

[77] C. Agodi, F. Bellini, G.a.P. Cirrone, F. Collamati, G. Cuttone, E.D. Lucia, M.D. Napoli, A.D. Domenico, R. Faccini, F. Ferroni, S. Fiore, P. Gauzzi, E. Iarocci, M. Marafini, I. Mattei, A. Paoloni, V. Patera, L. Piersanti, F. Romano, A. Sarti, A. Sciubba, C. Voena, Precise measurement of prompt photon emission from 80 MeV/u carbon ion beam irradiation, J. Instrum. 7 (03) (2012) P03001. http://dx.doi.org/10.1088/1748-0221/7/03/P03001.

[78] C. Agodi, F. Bellini, G.A.P. Cirrone, F. Collamati, G. Cuttone, E.D. Lucia, M.D. Napoli, A.D. Domenico, R. Faccini, F. Ferroni, S. Fiore, P. Gauzzi, E. Iarocci, M. Marafini, I. Mattei, A. Paoloni, V. Patera, L. Piersanti, F. Romano, A. Sarti, A. Sciubba, C. Voena, Erratum: Precise measurement of prompt photon emission from 80 MeV/u carbon ion beam irradiation, J. Instrum. 8 (11) (2013) E11002. http://dx.doi.org/10.1088/1748-0221/8/11/E11002.

[79] I. Mattei, G. Battistoni, F. Bini, F. Collamati, E.D. Lucia, M. Durante, R. Faccini, C.L. Tessa, M. Marafini, L. Piersanti, M. Rovituso, A. Rucinski, A. Russomando, A. Sarti, C. Schuy, A. Sciubba, E.S. Camillocci, M. Toppi, G. Traini, M. Vanstalle, C. Voena, V. Patera, Prompt-γ production of 220 MeV/u ^{12}C ions interacting with a PMMA target, J. Instrum. 10 (10) (2015) P10034. http://dx.doi.org/10.1088/1748-0221/10/10/P10034.

[80] I. Mattei, F. Collamati, E. De Lucia, R. Faccini, P.M. Frallicciardi, C. Mancini-Terracciano, M. Marafini, S. Muraro, R. Paramatti, V. Patera, L. Piersanti, D. Pinci, A. Rucinski, A. Russomando, A. Sarti, A. Sciubba, E.S. Camillocci, M. Toppi, G. Traini, C. Voena, G. Battistoni, Secondary radiation measurements for particle therapy applications: prompt photons produced by ^{4}He, ^{12}C and ^{16}O ion beams in a PMMA target, Phys. Med. Biol. 62 (4) (2017) 1438–1455. http://dx.doi.org/10.1088/1361-6560/62/4/1438. arXiv:1605.08377.

[81] M. Pinto, M. De Rydt, D. Dauvergne, G. Dedes, N. Freud, J. Krimmer, J.M. Létang, C. Ray, E. Testa, M. Testa, Technical Note: Experimental carbon ion range verification in inhomogeneous phantoms using prompt gammas, Med. Phys. 42 (5) (2015) 2342–2346. http://dx.doi.org/10.1118/1.4917225.

[82] J.M. Verburg, K. Riley, T. Bortfeld, J. Seco, Energy- and time-resolved detection of prompt gamma-rays for proton range verification, Phys. Med. Biol. 58 (20) (2013) L37. http://dx.doi.org/10.1088/0031-9155/58/20/L37.

[83] C. Min, J. Kim, M. Youn, C. Kim, Determination of distal dose edge location by measuring right-angled prompt-gamma rays from a 38 MeV proton beam, Nucl. Instrum. Methods Phys. Res. A 580 (1) (2007) 562–565. http://dx.doi.org/10.1016/j.nima.2007.05.235. Proceedings of the 10th International Symposium on Radiation Physics, ISRP 10.

[84] E. Testa, M. Bajard, M. Chevallier, D. Dauvergne, F.L. Foulher, N. Freud, J. Létang, J. Poizat, C. Ray, M. Testa, Dose profile monitoring with carbon ions by means of prompt-gamma measurements, Nucl. Instrum. Methods Phys. Res. B 267 (6) (2009) 993–996. http://dx.doi.org/10.1016/j.nimb.2009.02.031. Proceedings of the Seventh International Symposium on Swift Heavy Ions in Matter.

[85] A.K. Biegun, E. Seravalli, P. Cambraia Lopes, I. Rinaldi, M. Pinto, D.C. Oxley, P. Dendooven, F. Verhaegen, K. Parodi, P. Crespo, D.R. Schaart, Time-of-flight neutron rejection to improve prompt gamma imaging for proton range verification: a simulation study, Phys. Med. Biol. 57 (20) (2012) 6429. http://dx.doi.org/10.1088/0031-9155/57/20/6429.

[86] M. Testa, Charged particle therapy, ion range verification, prompt radiation, Université Claude Bernard - Lyon I, 2010, (Ph.D. thesis), http://tel.archives-ouvertes.fr/tel-00566188.

[87] C.H. Min, H.R. Lee, C.H. Kim, S.B. Lee, Development of array-type prompt gamma measurement system for in vivo range verification in proton therapy, Med. Phys. 39 (4) (2012) 2100–2107. http://dx.doi.org/10.1118/1.3694098.

[88] M. Pinto, D. Dauvergne, N. Freud, J. Krimmer, J.M. Letang, C. Ray, F. Roellinghoff, E. Testa, Design optimisation of a TOF-based collimated camera prototype for online hadrontherapy monitoring, Phys. Med. Biol. 59 (24) (2014) 7653–7674. http://dx.doi.org/10.1088/0031-9155/59/24/7653.

[89] J. Smeets, Prompt gamma imaging with a slit camera for real time range control in particle therapy, Ecole Polytechnique de Bruxelles, 2012 (Ph.D. thesis).

[90] D. Kim, H. Yim, J.-W. Kim, Pinhole camera measurements of prompt gamma-rays for detection of beam range variation in proton therapy, J. Korean Phys. Soc. 55 (4) (2009) 1673–1676. http://dx.doi.org/10.3938/jkps.55.1673.

[91] V. Bom, L. Joulaeizadeh, F. Beekman, Real-time prompt gamma monitoring in spot-scanning proton therapy using imaging through a knife-edge-shaped slit, Phys. Med. Biol. 57 (2) (2012) 297. http://dx.doi.org/10.1088/0031-9155/57/2/297.

[92] J. Smeets, F. Roellinghoff, D. Prieels, F. Stichelbaut, A. Benilov, P. Busca, C. Fiorini, R. Peloso, M. Basilavecchia, T. Frizzi, J.C. Dehaes, A. Dubus, Prompt gamma imaging with a slit camera for real-time range control in proton therapy, Phys. Med. Biol. 57 (11) (2012) 3371–3405. http://dx.doi.org/10.1088/0031-9155/57/11/3371.

[93] I. Perali, A. Celani, L. Bombelli, C. Fiorini, F. Camera, E. Clementel, S. Henrotin, G. Janssens, D. Prieels, F. Roellinghoff, J. Smeets, F. Stichelbaut, F.V. Stappen, Prompt gamma imaging of proton pencil beams at clinical dose rate, Phys. Med. Biol. 59 (19) (2014) 5849. http://dx.doi.org/10.1088/0031-9155/59/19/5849.

[94] M. Priegnitz, S. Helmbrecht, G. Janssens, I. Perali, J. Smeets, F.V. Stappen, E. Sterpin, F. Fiedler, Measurement of prompt gamma profiles in inhomogeneous targets with a knife-edge slit camera during proton irradiation, Phys. Med. Biol. 60 (12) (2015) 4849. http://dx.doi.org/10.1088/0031-9155/60/12/4849.

[95] M. Priegnitz, S. Barczyk, L. Nenoff, C. Golnik, I. Keitz, T. Werner, S. Mein, J. Smeets, F.V. Stappen, G. Janssens, L. Hotoiu, F. Fiedler, D. Prieels, W. Enghardt, G. Pausch, C. Richter, Towards clinical application: prompt gamma imaging of passively scattered proton fields with a knife-edge slit camera, Phys. Med. Biol. 61 (22) (2016) 7881. http://dx.doi.org/10.1088/0031-9155/61/22/7881.

[96] M. Priegnitz, S. Helmbrecht, G. Janssens, I. Perali, J. Smeets, F.V. Stappen, E. Sterpin, F. Fiedler, Detection of mixed-range proton pencil beams with a prompt gamma slit camera, Phys. Med. Biol. 61 (2) (2016) 855. http://dx.doi.org/10.1088/0031-9155/61/2/855.

[97] C. Richter, G. Pausch, S. Barczyk, M. Priegnitz, I. Keitz, J. Thiele, J. Smeets, F.V. Stappen, L. Bombelli, C. Fiorini, L. Hotoiu, I. Perali, D. Prieels, W. Enghardt, M. Baumann, First clinical application of a prompt gamma based in vivo proton range verification system, Radiother. Oncol. 118 (2) (2016) 232–237. http://dx.doi.org/10.1016/j.radonc.2016.01.004.

[98] Y. Xie, H. Bentefour, G. Janssens, J. Smeets, F.V. Stappen, L. Hotoiu, L. Yin, D. Dolney, S. Avery, F. O'Grady, D. Prieels, J. McDonough, T.D. Solberg, R. Lustig, A. Lin, B.-K.K. Teo, Prompt gamma imaging for in vivo range verification of pencil beam scanning proton therapy, Int. J. Radiat. Oncol. Biol. Phys. 0 (0) (2017). http://dx.doi.org/10.1016/j.ijrobp.2017.04.027.

[99] J. Ready, V. Negut, L. Mihailescu, K. Vetter, Prompt gamma imaging with a multi-knife-edge slit collimator: Evaluation for use in proton beam range verification, Med. Phys. 43 (6) (2016) 3717. http://dx.doi.org/10.1118/1.4957338.

[100] D. Everett, J. Fleming, R. Todd, J. Nightingale, Gamma-radiation lowercaseimaging system based on the Compton effect, Proc. Inst. Electr. Eng. 124 (11) (1977) 995. http://dx.doi.org/10.1049/piee.1977.0203.

[101] D. Xu, Z. He, Gamma-ray energy-imaging integrated spectral deconvolution, Nucl. Instrum. Methods Phys. Res. A 574 (1) (2007) 98–109. http://dx.doi.org/10.1016/j.nima.2007.01.171.

[102] E. Draeger, D. Mackin, S. Peterson, H. Chen, S. Beddar, J. Polf, A method to improve the spatial resolution of prompt gamma based Compton imaging for proton range verification, Med. Phys. 43 (6) (2016) 3451. http://dx.doi.org/10.1118/1.4956097.

[103] F. Roellinghoff, M.-H. Richard, M. Chevallier, J. Constanzo, D. Dauvergne, N. Freud, P. Henriquet, F. Le Foulher, J. Létang, G. Montarou, C. Ray, E. Testa, M. Testa, A. Walenta, Design of a Compton camera for 3D prompt-gamma imaging during ion beam therapy, Nucl. Instrum. Methods Phys. Res. A 648 (Supplement 1) (2011) S20–S23. http://dx.doi.org/10.1016/j.nima.2011.01.069.

[104] G. Llosá, J. Barrio, J. Cabello, A. Crespo, C. Lacasta, M. Rafecas, S. Callier, C. de La Taille, L. Raux, Detector characterization and first coincidence tests of a Compton telescope based on LaBr3 crystals and SiPMs, Nucl. Instrum. Methods Phys. Res. A 695 (0) (2012) 105–108. http://dx.doi.org/10.1016/j.nima.2011.11.041.

[105] Z. Li, M. Wedrowski, P. Bruyndonckx, G. Vandersteen, Nonlinear least-squares modeling of 3D interaction position in a monolithic scintillator block, Phys. Med. Biol. 55 (21) (2010) 6515. http://dx.doi.org/10.1088/0031-9155/55/21/012.

[106] G. Llosá, J. Cabello, S. Callier, J. Gillam, C. Lacasta, M. Rafecas, L. Raux, C. Solaz, V. Stankova, C. de La Taille, M. Trovato, J. Barrio, First Compton telescope prototype based on continuous LaBr3-SiPM detectors, Nucl. Instrum. Methods Phys. Res. A 718 (2013) 130–133. http://dx.doi.org/10.1016/j.nima.2012.08.074.

[107] G. Llosá, M. Trovato, J. Barrio, A. Etxebeste, E.M. noz, C. Lacasta, J.F. Oliver, M. Rafecas, C. Solaz, P. Solevi, First images of a three-layer Compton telescope prototype for treatment monitoring in hadron therapy, Front. Oncol. 6 (2016) 14. http://dx.doi.org/10.3389/fonc.2016.00014.

[108] P. Solevi, E. Muñoz, C. Solaz, M. Trovato, P. Dendooven, J.E. Gillam, Carlos Lacasta, J.F. Oliver, M. Rafecas, I. Torres-Espallardo, G. Llosá, Performance of MACACO Compton telescope for ion-beam therapy monitoring: first test with proton beams,

Phys. Med. Biol. 61 (14) (2016) 5149. http://dx.doi.org/10.1088/0031-9155/61/14/5149.

[109] A. Kishimoto, J. Kataoka, T. Nishiyama, T. Taya, S. Kabuki, Demonstration of three-dimensional imaging based on handheld Compton camera, J. Instrum. 10 (11) (2015) P11001. http://dx.doi.org/10.1088/1748-0221/10/11/P11001.

[110] T. Taya, J. Kataoka, A. Kishimoto, Y. Iwamoto, A. Koide, T. Nishio, S. Kabuki, T. Inaniwa, First demonstration of real-time gamma imaging by using a handheld compton camera for particle therapy, Nucl. Instrum. Methods Phys. Res. A 831 (2016) 355–361. http://dx.doi.org/10.1016/j.nima.2016.04.028. Proceedings of the 10th International Hiroshima Symposium on the Development and Application of Semiconductor Tracking Detectors.

[111] M.-H. Richard, M. Chevallier, D. Dauvergne, N. Freud, P. Henriquet, F. Le Foulher, J. Létang, G. Montarou, C. Ray, F. Roellinghoff, E. Testa, M. Testa, A. Walenta, Design guidelines for a double scattering Compton camera for prompt-gamma imaging during ion beam therapy: A Monte Carlo simulation study, IEEE Trans. Nucl. Sci. 58 (1) (2011) 87–94. http://dx.doi.org/10.1109/NSSMIC.2011.6152642.

[112] M.-H. Richard, M. Dahoumane, D. Dauvergne, M. De Rydt, G. Dedes, N. Freud, J. Krimmer, J. Létang, X. Lojacono, V. Maxim, G. Montarou, C. Ray, F. Roellinghoff, E. Testa, A. Walenta, Design study of the absorber detector of a Compton camera for on-line control in ion beam therapy, IEEE Trans. Nucl. Sci. 59 (5) (2012) 1850–1855. http://dx.doi.org/10.1109/TNS.2012.2206053.

[113] C. Abellan, J.P. Cachemiche, F. Réthoré, C. Morel, A data acquisition system for medical imaging, in: 3rd International Conference on Advancements in Nuclear Instrumentation, Measurement Methods and their Applications (ANIMMA), 2013, pp. 1–7. http://dx.doi.org/10.1109/ANIMMA.2013.6728028.

[114] S. Deng, H. Mathez, D. Dauvergne, Y. Zoccarato, G.-N. Lu, Front-end multi-channel PMT-associated readout chip for hodoscope application, Nucl. Instrum. Methods Phys. Res. A 695 (2012) 390–393. http://dx.doi.org/10.1016/j.nima.2011.11.042.

[115] M. Dahoumane, D. Dauvergne, J. Krimmer, J.L. Ley, E. Testa, Y. Zoccarato, A low noise and high dynamic range CMOS integrated Electronics associated with double sided Silicon Strip Detectors for a Compton camera gamma-ray detecting system, in: IEEE Nuclear Science Symposium and Medical Imaging Conference (NSS/MIC), 2014, pp. 1–6. http://dx.doi.org/10.1109/NSSMIC.2014.7431122.

[116] J. Krimmer, J.-L. Ley, C. Abellan, J.-P. Cachemiche, L. Caponetto, X. Chen, M. Dahoumane, D. Dauvergne, N. Freud, B. Joly, D. Lambert, L. Lestand, J.M. Létang, M. Magne, H. Mathez, V. Maxim, G. Montarou, C. Morel, M. Pinto, C. Ray, V. Reithinger, E. Testa, Y. Zoccarato, Development of a Compton camera for medical applications based on silicon strip and scintillation detectors, Nucl. Instrum. Methods Phys. Res. A 787 (0) (2015) 98–101. http://dx.doi.org/10.1016/j.nima.2014.11.042. New Developments in Photodetection {NDIP14}.

[117] M. Frandes, A. Zoglauer, V. Maxim, R. Prost, A tracking Compton-scattering imaging system for hadron therapy monitoring, IEEE Trans. Nucl. Sci. 57 (1) (2010) 144–150. http://dx.doi.org/10.1109/TNS.2009.2031679.

[118] P. Thirolf, C. Lang, S. Aldawood, H.v.d. Kolff, L. Maier, D. Schaart, K. Parodi, Development of a Compton camera for online range monitoring of laser-accelerated proton beams via prompt-gamma detection, in: S. Lunardi, P. Bizzeti, C. Bucci, M. Chiari, A. Dainese, P. Di Nezza, R. Menegazzo, A. Nannini, C. Signorini, J. Valiente-Dobon (Eds.), EPJ Web Conf. 66 (2014) 11036. http://dx.doi.org/10.1051/epjconf/20146611036.

[119] H.T. Van Dam, S. Seifert, R. Vinke, P. Dendooven, H. Lohner, F.J. Beekman, D.R. Schaart, Improved nearest neighbor methods for gamma photon interaction position determination in monolithic scintillator PET detectors, IEEE Trans. Nucl. Sci. 58 (5) (2011) 2139–2147. http://dx.doi.org/10.1109/TNS.2011.2150762.

[120] P. Thirolf, S. Aldawood, M. Böhmer, J. Bortfeldt, I. Castelhano, G. Dedes, F. Fiedler, R. Gernhäuser, C. Golnik, S. Helmbrecht, F. Hueso-González, H. v. Kolff, T. Kormoll, C. Lang, S. Liprandi, R. Lutter, T. Marinšek, L. Maier, G. Pausch, J. Petzoldt, K. Römer, D. Schaart, K. Parodi, A Compton camera prototype for prompt gamma medical imaging, in: V. Greco, M. La Cognata, S. Pirrone, F. Rizzo, C. Spitaleri (Eds.), EPJ Web Conf. 117 (2016) 05005. http://dx.doi.org/10.1051/epjconf/201611705005.

[121] C. Lang, D. Habs, K. Parodi, P.G. Thirolf, Sub-millimeter nuclear medical imaging with high sensitivity in positron emission tomography using $\beta^+\gamma$ coincidences, J. Instrum. 9 (01) (2014) P01008. http://dx.doi.org/10.1088/1748-0221/9/01/P01008.

[122] T. Kormoll, F. Fiedler, S. Schöne, J. Wüstemann, K. Zuber, W. Enghardt, A Compton imager for in-vivo dosimetry of proton beams — design study, Nucl. Instrum. Methods Phys. Res. A 626–627 (0) (2011) 114–119. http://dx.doi.org/10.1016/j.nima.2010.10.031.

[123] F. Hueso-González, C. Golnik, M. Berthel, A. Dreyer, W. Enghardt, F. Fiedler, K. Heidel, T. Kormoll, H. Rohling, S. Schöne, R. Schwengner, A. Wagner, G. Pausch, Test of Compton camera components for prompt gamma imaging at the ELBE Bremsstrahlung beam, J. Instrum. 9 (05) (2014) P05002. http://dx.doi.org/10.1088/1748-0221/9/05/P05002.

[124] F. Hueso-González, A. Biegun, P. Dendooven, W. Enghardt, F. Fiedler, C. Golnik, K. Heidel, T. Kormoll, J. Petzoldt, K. Römer, R. Schwengner, A. Wagner, G. Pausch, Comparison of LSO and BGO block detectors for prompt gamma imaging in ion beam therapy, J. Instrum. 10 (09) (2015) P09015. http://dx.doi.org/10.1088/1748-0221/10/09/P09015.

[125] Q. Wei, X. Li, T. Ma, S. Wang, T. Dai, P. Fan, Y. Yu, Y. Jin, Y. Liu, A neighborhood standard deviation based algorithm for generating PET crystal position maps, in: 2013 IEEE Nuclear Science Symposium and Medical Imaging Conference (2013 NSS/MIC), 2013, pp. 1–4. http://dx.doi.org/10.1109/NSSMIC.2013.6829273.

[126] C. Golnik, D. Bemmerer, W. Enghardt, F. Fiedler, F. Hueso-González, G. Pausch, K. Römer, H. Rohling, S. Schöne, L. Wagner, T. Kormoll, Tests of a Compton imaging prototype in a monoenergetic 4.44 MeV photon field — a benchmark setup for prompt gamma-ray imaging devices, J. Instrum. 11 (06) (2016) P06009. http://dx.doi.org/10.1088/1748-0221/11/06/P06009.

[127] C.H. Kim, J.H. Park, H. Seo, H.R. Lee, Erratum: Gamma electron vertex imaging and application to beam range verification in proton therapy, Med. Phys. 39 (10) (2012) 6523–6524. http://dx.doi.org/10.1118/1.4749930.

[128] H.R. Lee, S.H. Kim, J.H. Park, W.G. Jung, H. Lim, C.H. Kim, Prototype system for proton beam range measurement based on gamma electron vertex imaging, Nucl. Instrum. Methods Phys. Res. A (2017). http://dx.doi.org/10.1016/j.nima.2017.03.022.

[129] S.W. Peterson, D. Robertson, J. Polf, Optimizing a three-stage compton camera for measuring prompt gamma rays emitted during proton radiotherapy, Phys. Med. Biol. 55 (22) (2010) 6841. http://dx.doi.org/10.1088/0031-9155/55/22/015.

[130] D. Robertson, J.C. Polf, S.W. Peterson, M.T. Gillin, S. Beddar, Material efficiency studies for a compton camera designed to measure characteristic prompt gamma rays emitted during proton beam radiotherapy, Phys. Med. Biol. 56 (10) (2011) 3047. http://dx.doi.org/10.1088/0031-9155/56/10/010.

[131] D. Mackin, J. Polf, S. Peterson, S. Beddar, The effects of Doppler broadening and detector resolution on the performance of three-stage Compton cameras, Med. Phys. 40 (1) (2013) 012402–n/a. http://dx.doi.org/10.1118/1.4767756. 012402.

[132] M. McCleskey, W. Kaye, D. Mackin, S. Beddar, Z. He, J. Polf, Evaluation of a multistage CdZnTe Compton camera for prompt gamma imaging for proton therapy, Nucl. Instrum. Methods Phys. Res. A 785 (2015) 163–169. http://dx.doi.org/10.1016/j.nima.2015.02.030.

[133] A. Takada, H. Kubo, H. Nishimura, K. Ueno, K. Hattori, S. Kabuki, S. Kurosawa, K. Miuchi, E. Mizuta, T. Nagayoshi, N. Nonaka, Y. Okada, R. Orito, H. Sekiya, A. Takeda, T. Tanimori, Observation of diffuse cosmic and atmospheric gamma rays at balloon altitudes with an electron-tracking compton camera, Astrophys. J. 733 (1) (2011) 13. http://dx.doi.org/10.1088/0004-637X/733/1/13.

[134] T. Tanimori, H. Kubo, K. Miuchi, T. Nagayoshi, Y. Okada, R. Orito, A. Takada, A. Takeda, Time projection chamber based on micro-pattern detector for neutron time-resolved imaging, Nucl. Instrum. Methods Phys. Res. A 529 (1) (2004) 373–377. http://dx.doi.org/10.1016/j.nima.2004.05.014. Proceedings of the Joint Meeting of the International Conference on Neutron Optics, NOP2004 and the Third International Workshop on Position-Sensitive Neutron Detectors, PSND2004.

[135] S. Kurosawa, H. Kubo, K. Ueno, S. Kabuki, S. Iwaki, M. Takahashi, K. Taniue, N. Higashi, K. Miuchi, T. Tanimori, D. Kim, J. Kim, Prompt gamma detection for range verification in proton therapy, Curr. Appl. Phys. 12 (2) (2012) 364–368. http://dx.doi.org/10.1016/j.cap.2011.07.027.

[136] M. Takahashi, S. Kabuki, K. Hattori, N. Higashi, S. Iwaki, H. Kubo, S. Kurosawa, K. Miuchi, K. Nakamura, H. Nishimura, J.D. Parker, T. Sawano, A. Takada, T. Tanimori, K. Taniue, K. Ueno, Development of an Electron-Tracking Compton Camera using CF4 gas at high pressure for improved detection efficiency, Nucl. Instrum. Methods Phys. Res. A 628 (1) (2011) 150–153. http://dx.doi.org/10.1016/j.nima.2010.06.305. VCI 2010, Proceedings of the 12th International Vienna Conference on Instrumentation.

[137] J.-L. Ley, Development of a time-of-flight Compton camera prototype for online control of ion therapy and medical imaging, Université Claude Bernard - Lyon I, 2015 (Ph.D. thesis). https://hal.archives-ouvertes.fr/tel-01280098.

[138] H. Rohling, M. Priegnitz, S. Schoene, A. Schumann, W. Enghardt, F. Hueso-González, G. Pausch, F. Fiedler, Requirements for a Compton camera for in vivo range verification of proton therapy, Phys. Med. Biol. 62 (7) (2017) 2795. http://dx.doi.org/10.1088/1361-6560/aa6068.

[139] F. Hueso-González, W. Enghardt, F. Fiedler, C. Golnik, G. Janssens, Johannes Petzoldt, D. Prieels, M. Priegnitz, K.E. Römer, J. Smeets, F.V. Stappen, Andreas Wagner, G. Pausch, First test of the prompt gamma ray timing method with heterogeneous targets at a clinical proton therapy facility, Phys. Med. Biol. 60 (16) (2015) 6247. http://dx.doi.org/10.1088/0031-9155/60/16/6247.

[140] J. Petzoldt, K.E. Roemer, W. Enghardt, F. Fiedler, C. Golnik, F. Hueso-González, S. Helmbrecht, T. Kormoll, HRohling, J. Smeets, T. Werner, G. Pausch, Characterization of the microbunch time structure of proton pencil beams at a clinical treatment facility, Phys. Med. Biol. 61 (6) (2016) 2432. http://dx.doi.org/10.1088/0031-9155/61/6/2432.

[141] G. Pausch, J. Petzoldt, M. Berthel, W. Enghardt, F. Fiedler, C. Golnik, F. Hueso-González, R. Lentering, K. Römer, K. Ruhnau, J. Stein, A. Wolf, T. Kormoll, Scintillator-based high-throughput fast timing spectroscopy for real-time range verification in particle therapy, IEEE Trans. Nucl. Sci. 63 (2) (2016) 664–672. http://dx.doi.org/10.1109/TNS.2016.2527822.

[142] A. Carnicer, V. Letellier, G. Rucka, G. Angellier, W. Sauerwein, J. Hérault, Study of the secondary neutral radiation in proton therapy: Toward an indirect in vivo dosimetry, Med. Phys. 39 (12) (2012) 7303–7316. http://dx.doi.org/10.1118/1.4765049.

[143] S. Goetsch, Patient safety and radiation accidents, in: San Diego Radiotherapy Workshops, 2013, http://sdradiotherapy.com/Packages.html.

[144] M. Testa, C.H. Min, J.M. Verburg, J. Schümann, H.-M. Lu, H. Paganetti, Range verification of passively scattered proton beams based on prompt gamma time patterns, Phys. Med. Biol. 59 (15) (2014) 4181. http://dx.doi.org/10.1088/0031-9155/59/15/4181.

[145] J.M. Verburg, M. Testa, J. Seco, Range verification of passively scattered proton beams using prompt gamma-ray detection, Phys. Med. Biol. 60 (3) (2015) 1019. http://dx.doi.org/10.1088/0031-9155/60/3/1019.

[146] J.C. Polf, S. Peterson, G. Ciangaru, M. Gillin, S. Beddar, Prompt gamma-ray emission from biological tissues during proton irradiation: a preliminary study, Phys. Med. Biol 54 (2009) 731–743. http://dx.doi.org/10.1088/0031-9155/54/3/017. 00061.

[147] J.C. Polf, S. Peterson, M. McCleskey, B.T. Roeder, A. Spiridon, S. Beddar, L. Trache, Measurement and calculation of characteristic prompt gamma ray spectra emitted during proton irradiation, Phys. Med. Biol. 54 (22) (2009) N519. http://dx.doi.org/10.1088/0031-9155/54/22/N02.

[148] J.C. Polf, R. Panthi, D.S. Mackin, M. McCleskey, A. Saastamoinen, B.T. Roeder, S. Beddar, Measurement of characteristic prompt gamma rays emitted from oxygen and carbon in tissue-equivalent samples during proton beam irradiation, Phys. Med. Biol. 58 (17) (2013) 5821. http://dx.doi.org/10.1088/0031-9155/58/17/5821.

[149] J. Smeets, F. Roellinghoff, G. Janssens, I. Perali, A. Celani, C. Fiorini, N. Freud, E. Testa, D. Prieels, Experimental comparison of knife-edge and multi-parallel slit collimators for prompt gamma imaging of proton pencil beams, Radiat. Oncol. (2016) 156. http://dx.doi.org/10.3389/fonc.2016.00156.

[150] H.-H. Lin, H.-T. Chang, T.-C. Chao, K.-S. Chuang, A comparison of two prompt gamma imaging techniques with collimator-based cameras for range verification in proton therapy, Radiat. Phys. Chem. (2016). http://dx.doi.org/10.1016/j.radphyschem.2016.04.020.

[151] P. Gueth, D. Dauvergne, N. Freud, J.M. Létang, C. Ray, E. Testa, D. Sarrut, Machine learning-based patient specific prompt-gamma dose monitoring in proton therapy, Phys. Med. Biol. 58 (13) (2013) 4563.

[152] C.P. Raaijmakers, M.W. Konijnenberg, L. Dewit, D. Haritz, R. Huiskamp, K. Philipp, A. Siefert, F. Stecher-Rasmussen, B.J. Mijnheer, Monitoring of blood- ^{10}B concentration for boron neutron capture therapy using prompt gamma-ray analysis, Acta Oncol. 34 (4) (1995) 517–523. http://dx.doi.org/10.3109/02841869509094017.

[153] H.-B. Shin, D.-K. Yoon, J.-Y. Jung, M.-S. Kim, T.S. Suh, Prompt gamma ray imaging for verification of proton boron fusion therapy: A Monte Carlo study, Phys. Med. 32 (10) (2016) 1271–1275. http://dx.doi.org/10.1016/j.ejmp.2016.05.053.

[154] G. Petringa, G.A.P. Cirrone, C. Caliri, G. Cuttone, L. Giuffrida, G.L. Rosa, R. Manna, L. Manti, V. Marchese, C. Marchetta, D. Margarone, G. Milluzzo, A. Picciotto, F. Romano, F.P. Romano, A.D. Russo, G. Russo, D. Santonocito, V. Scuderi, Prompt gamma-ray emission for future imaging applications in proton-boron fusion therapy, J. Instrum. 12 (03) (2017) C03059. http://dx.doi.org/10.1088/1748-0221/12/03/C03059.

[155] W. Enghardt, P. Crespo, F. Fiedler, R. Hinz, K. Parodi, J. Pawelke, F. Pönisch, Charged hadron tumour therapy monitoring by means of PET, Nucl. Instrum. Methods Phys. Res. A 525 (1–2) (2004) 284–288. http://dx.doi.org/10.1016/j.nima.2004.03.128.

[156] M. Marafini, A. Attili, G. Battistoni, N. Belcari, M. Bisogni, N. Camarlinghi, F. Cappucci, M. Cecchetti, P. Cerello, F. Ciciriello, G. Cirrone, S. Coli, F. Corsi, G. Cuttone, E. De Lucia, S. Ferretti, R. Faccini, E. Fiorina, P. Fralliccardi, G. Giraudo, E. Kostara, A. Kraan, F. Licciulli, B. Liu, N. Marino, C. Marzocca, G. Matarrese, C. Morone, M. Morrocchi, S. Muraro, V. Patera, F. Pennazio, C. Peroni, L. Piersanti, M. Piliero, G. Pirrone, A. Rivetti, F. Romano, V. Rosso, P. Sala, A. Sarti, A. Sciubba, G. Sportelli, C. Voena, R. Wheadon, A. Del Guerra, The INSIDE Project: Innovative solutions for in-beam dosimetry in hadrontherapy, Acta Phys. Polon. A 127 (5) (2015) 1465–1467. http://dx.doi.org/10.12693/APhysPolA.127.1465.

[157] P.C. Lopes, J. Bauer, A. Salomon, I. Rinaldi, V. Tabacchini, T. Tessonnier, P. Crespo, K. Parodi, D. Schaart, First in situ TOF-PET study using digital photon counters for proton range verification, Phys. Med. Biol. 61 (16) (2016) 6203. http://dx.doi.org/10.1088/0031-9155/61/16/6203.

[158] H. Tashima, T. Yamaya, E. Yoshida, S. Kinouchi, M. Watanabe, E. Tanaka, A single-ring OpenPET enabling PET imaging during radiotherapy, Phys. Med. Biol. 57 (14) (2012) 4705. http://dx.doi.org/10.1088/0031-9155/57/14/4705.

[159] H. Tashima, E. Yoshida, N. Inadama, F. Nishikido, Y. Nakajima, H. Wakizaka, T. Shinaji, M. Nitta, S. Kinouchi, M. Suga, et al., Development of a small single-ring OpenPET prototype with a novel transformable architecture, Phys. Med. Biol. 61 (4) (2016) 1795. http://dx.doi.org/10.1088/0031-9155/61/4/1795.

[160] P. Dendooven, H. Buitenhuis, F. Diblen, P. Heeres, A. Biegun, F. Fiedler, M. van Goethem, E. van der Graaf, S. Brandenburg, Short-lived positron emitters in beam-on PET imaging during proton therapy, Phys. Med. Biol. 60 (23) (2015) 8923. http://dx.doi.org/10.1088/0031-9155/60/23/8923.

[161] M. Bucciantonio, U. Amaldi, R. Kieffer, F. Sauli, D. Watts, Development of a fast proton range radiography system for quality assurance in hadrontherapy, Nucl. Instrum. Methods Phys. Res. A (2013). http://dx.doi.org/10.1016/j.nima.2013.05.110.

[162] L. Piersanti, F. Bellini, F. Bini, F. Collamati, E.D. Lucia, M. Durante, R. Faccini, F. Ferroni, S. Fiore, E. Iarocci, C.L. Tessa, M. Marafini, I. Mattei, V. Patera, P.G. Ortega, A. Sarti, C. Schuy, A. Sciubba, M. Vanstalle, C. Voena, Measurement of charged particle yields from PMMA irradiated by a 220 MeV/u ^{12}C beam, Phys. Med. Biol. 59 (7) (2014) 1857. http://dx.doi.org/10.1088/0031-9155/59/7/1857.

[163] G. Battistoni, F. Collamati, E. De Lucia, R. Faccini, M. Marafini, I. Mattei, S. Muraro, R. Paramatti, V. Patera, D. Pinci, A. Rucinski, A. Russomando, A. Sarti, A. Sciubba, E. Solfaroli Camillocci, M. Toppi, G. Traini, C. Voena, Design of a tracking device for on-line dose monitoring in hadrontherapy, Nucl. Instrum. Methods Phys. Res. A 845 (2017) 679–683. http://dx.doi.org/10.1016/j.nima.2016.05.095.

[164] R. Rescigno, J. Baudot, S. Brons, D. Dauvergne, C. Finck, D. Juliani, J. Krimmer, K. Parodi, C. Ray, V. Reithinger, I. Rinaldi, M. Rousseau, E. Testa, M. Winter, Proton interaction vertex imaging for carbon therapy quality control, Radiother. Oncol. 110 (2014) S81–S82. http://dx.doi.org/10.1016/S0167-8140(15)34187-6.

[165] A.M. Reinhart, C.K. Spindeldreier, J. Jakubek, M. Martišíková, Three dimensional reconstruction of therapeutic carbon ion beams in phantoms using single secondary ion tracks, Phys. Med. Biol. 62 (12) (2017) 4884. http://dx.doi.org/10.1088/1361-6560/aa6aeb.

[166] J. Bauer, F. Sommerer, A. Mairani, D. Unholtz, R. Farook, J. Handrack, K. Frey, T. Marcelos, T. Tessonnier, S. Ecker, B Ackermann, M. Ellerbrock, J. Debus, K. Parodi, Integration and evaluation of automated Monte Carlo simulations in the clinical practice of scanned proton and carbon ion beam therapy, Phys. Med. Biol. 59 (16) (2014) 4635. http://dx.doi.org/10.1088/0031-9155/59/16/4635.

[167] H. Spreeuw, R. Rozendaal, I. Olaciregui-Ruiz, P. González, A. Mans, B. Mijnheer, M. van Herk, Online 3D EPID-based dose verification: Proof of concept, Med. Phys. 43 (7) (2016) 3969–3974. http://dx.doi.org/10.1118/1.4952729.

[168] S. Remmele, J. Hesser, H. Paganetti, T. Bortfeld, A deconvolution approach for PET-based dose reconstruction in proton radiotherapy, Phys. Med. Biol. 56 (23) (2011) 7601–7619. http://dx.doi.org/10.1088/0031-9155/56/23/017.

[169] K. Parodi, On- and off-line monitoring of ion beam treatment, Nucl. Instrum. Methods Phys. Res. A (2016). http://dx.doi.org/10.1016/j.nima.2015.06.056.

[170] V. Ferrero, The INSIDE project: in-beam PET scanner system features and characterization, J. Instrum. 12 (03) (2017) C03051. http://dx.doi.org/10.1088/1748-0221/12/03/C03051.

[171] M.-L. Gallin-Martel, A. Bes, A. Boukhémiri, G. Bosson, J. Collot, D. Dauvergne, M. Fontana, L. Gallin-Martel, A. Gorecki, J. Hostachy, J. Krimmer, A. Lacoste, S. Marcatili, J. Morse, J.-F. Muraz, F. Rarbi, O. Rossetto, M. Salomé, E. Testa, M. Yamouni, Large area polycrystalline diamond detectors for online hadron therapy beam tagging applications, in: IEEE Nuclear Science Symposium & Medical Imaging Conference, 2016 IEEE NSS/MIC, IEEE, 2016. https://hal.archives-ouvertes.fr/hal-01436786.